AERODYNAMIC PRELIMINARY ANALYSIS SYSTEM

PART I THEORY

BY

E. BONNER, W. CLEVER, K. DUNN

PREPARED UNDER CONTRACT NAS1-14686
BY LOS ANGELES DIVISION
ROCKWELL INTERNATIONAL
LOS ANGELES, CALIFORNIA

FOR

LANGLEY RESEARCH CENTER
NATIONAL AERONAUTICS AND SPACE ADMINISTRATION

AERODYNAMIC PRELIMINARY ANALYSIS SYSTEM

PART I THEORY

By E. Bonner, W. Clever, K. Dunn

Los Angeles Division, Rockwell International

SUMMARY

A comprehensive aerodynamic analysis program based on linearized potential theory is described. The solution treats thickness and attitude problems at subsonic and supersonic speeds. Three dimensional configurations with or without jet flaps having multiple non-planar surfaces of arbitrary planform and open or closed slender bodies of non-circular contour may be analyzed. Longitudinal and lateral-directional static and rotary derivative solutions may be generated.

The analysis has been implemented on a time sharing system in conjunction with an input tablet digitizer and an interactive graphics input/output display and editing terminal to maximize its responsiveness to the preliminary analysis problem. Nominal case computation time of 45 CPU seconds on the CDC 175 for a 200 panel simulation indicates the program provides an efficient analysis for systematically performing various aerodynamic configuration tradeoff and evaluation studies.

TABLE OF CONTENTS

INTRODUCTION

Computerization of aerodynamic theory has developed to a point where the analysis of complete aircraft configurations by a single program is now possible. Programs designed for this purpose in fact currently exist, but are limited in scope and abound with subtleties requiring the user to be highly experienced. Many of the difficulties are attributable to the level of precision of the underlying theory and the numerical sensitivity of the associated solution. In preliminary design stages, it is often desirable to accept some degree of approximation in the interest of modest turn-around time, reduced computational costs, simplification of input, and stability and generality of results. The importance of short elapsed time stems from the necessity to survey systematically a large number of candidate advanced configurations or major component geometric parameters for a set of overall system requirements in a timely manner. Modest computational cost allows a greater number of configurations and/or conditions to be economically investigated.

One approach in this spirit is to replace the commonly employed exact superposition method, which panels the entire aircraft surface, with approximations involving linearized boundary conditions and solutions of a local two-dimensional potential equation. In the exact theories, a determination of the singularity strengths required to satisfy boundary conditions leads to the necessity of inverting very large matrices. The nature of the approximate linearized theories on the other hand substantially reduces the number of simultaneous equations encountered and consequently places far less demand upon computer capabilities.

Linearized theory when combined with realistic assessments of limitations and estimated viscous characteristics provides a valuable tool for analyzing general aircraft configurations and aerodynamic interactions at modest attitudes for both subsonic and supersonic speeds.

LIST OF SYMBOLS

A	Projected oblique cross section area
A_{ij}	Influence coefficient. Normalwash at control point i due to vortex panel j of unit strength
A_i	Area of quadrilateral panel i
$\mathcal{A}_{ij}$	Coefficients in the set of linear equations for the vortex panel strengths
b	Reference span
c	Local chord
$\bar{c}$	Reference chord
c_{AVG}	Average chord
C_d	Section drag coefficient
C_D	Drag coefficient
C_{D_F}	Flat plate skin friction drag coefficient
C_{DMIN}	Minimum drag due to lift
C_F	Flat plate skin friction drag coefficient
C_i	Boundary condition for control point i
C_ℓ	Section lift coefficient
C_ℓ, C_m, C_n	Roll, pitch and yaw moment coefficients
C_L	Lift coefficient
C_n	Section normal coefficient
C_P	Pressure coefficient $(P-P_\infty)/q$
$C_{P_{NET}}$	Net pressure coefficient $(P_\ell-P_u)/q$ and vortex panel strength
C_Y	Side force coefficient

LIST OF SYMBOLS (CONTINUED)

C_μ	Section momentum coefficient mV/qc
C^*	$\frac{\mu^*}{\mu_\infty}\frac{T_\infty}{T_\infty}$
D	Drag
F	Jet reaction force
F_X, F_Y, F_Z	Force components for body of unit length
g(x)	Axisymmetric outer solution to potential equation
h	Radius of curvature of cross sectional boundary
$\bar{i}, \bar{j}, \bar{k}$	Unit vectors in x,y,z direction respectively
K	Drag due to lift factor or skin friction thickness correction factor
K_S	Equivalent distributed sand gain height
ℓ	Effective length
$\ell(i,n)$	Length of segment i, i+1 of contour C_n
$\bar{L}$	Equivalent body length or geometric length
L/d	Body fineness ratio
m	Mass rate of flow
M	Mach number
M_X, M_Y, M_Z	Moment components for body of unit length
n	Unit normal
p,q,r	Rolling, pitching and yawing velocity about x, y and z
$\hat{p}, \hat{q}, \hat{r}$	Nondimensional angular velocities pb/2U, $q\bar{c}$/2U and rb/2U
P	Pressure
P_r	Prandtl number

LIST OF SYMBOLS (CONTINUED)

q	Free stream dynamic pressure $1/2\rho U^2$
r	Recovery factor
R	Unit Reynolds number or radius of curvature
$R_{[\ ]}$	Reynolds number based on [ ]
$\mathcal{R}$	Gas constant
s	Segment arc length
S	Body cross sectional area or surface area
S_{REF}	Reference area
T	Static temperature -°R or tangent of quadrilateral panel leading edge sweep
t/c	Airfoil thickness ratio
u,v,w	x,y,z nondimensional components of perturbation velocity
U	Freestream velocity
V	Jet velocity
W	Complex potential function
x,y,z	Body axis coordinate system
x,r,θ	Cylindrical coordinate system
Z	Complex number y+iz
α	Angle of attack
α_i	Local angle of attack at surface control point i
β	Angle of sideslip or $\sqrt{\lvert 1-M^2 \rvert}$

LIST OF SYMBOLS (CONTINUED)

γ	Vorticity strength per unit length or ratio of specific heats
Γ	Horseshoe vortex strength in Trefftz plane
δ	Control surface deflection
δ_{ij}	Kroneker delta 0 $i \neq j$ 1 $i=j$
δ_j	Jet deflection angle relative to trailing edge
δ_{jT}	Total jet deflection angle
$\frac{\delta \nu}{\delta x}$	Body slope
$\Delta\phi$	Arc of jet segment
θ	Dihedral angle of quadrilateral panel or boundary layer momentum thickness
μ	Absolute viscosity
ν	Kinematic viscosity, μ/ρ
ρ	Density
σ	Source density
ϕ	Perturbation velocity potential
Φ	Total velocity potential
ψ	See figure 3
Subscript	
c	camber
CG	center of gravity
u	upper surface

ℓ	lower surface
LE	leading edge
r	recovery
t	thickness
TRAN	transition point
∞	freestream condition

Superscript

'	quantity based on effective origin
*	Eckert reference temperature condition

THEORY

The arbitrary configurations which may be treated by the analysis are simulated by a distribution of source and vortex singularities. Each of these singularities satisfies the linearized small perturbation potential equation of motion

$$\beta^2 \phi_{xx} + \phi_{yy} + \phi_{zz} = 0$$

The singularity strengths are obtained by satisfying the condition that the flow is tangent to the local surface:

$$\frac{\partial \Phi}{\partial n} = 0$$

All of the resulting velocities and pressures throughout the flow may be obtained when the singularity strengths are known. A configuration is composed of bodies, interference shells and aerodynamic surfaces (wings, canards, tails etc.). The following types of singularites are used to represent each.

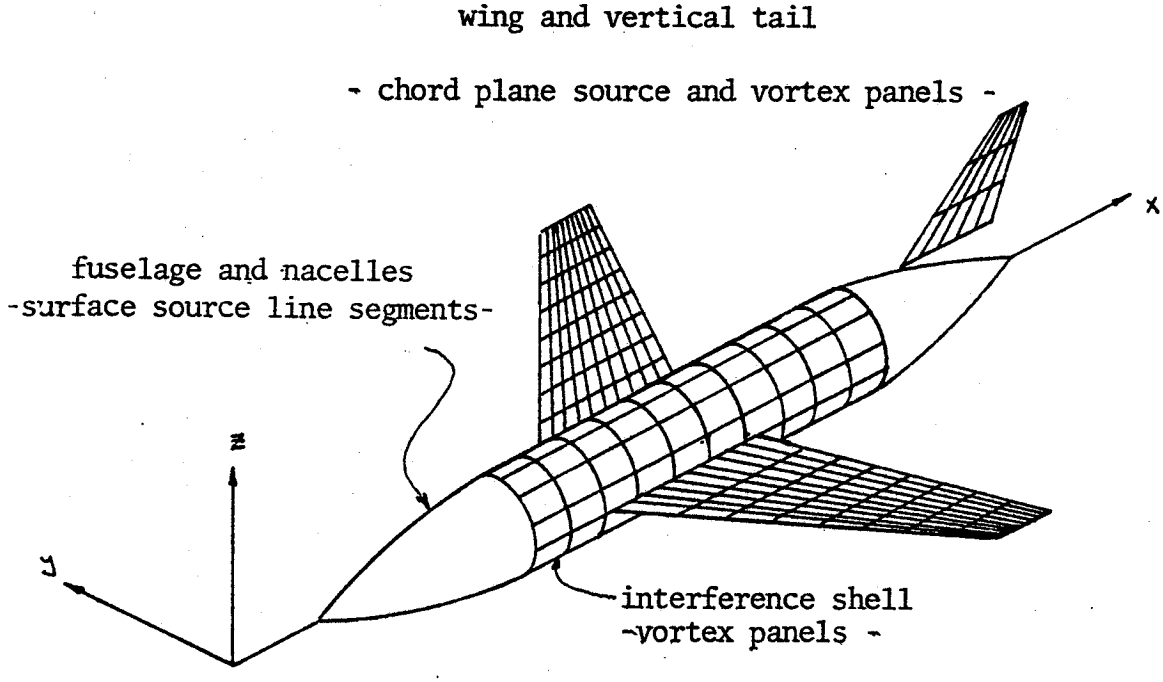

The first step in the solution procedure consists of obtaining the strengths of the singularities simulating the fuselage and nacelles, from an isolated body solution. The present analysis uses slender body theory to

predict the surface and near field properties. The solution is composed of a compressible axisymmetric component for a body of revolution of the same crossectional area and an incompressible crossflow component, ϕ, satisfying the local three dimensional boundary conditions in the (y,z) plane. The crossflow is a solution of Laplace's equation

$$\phi_{yy} + \phi_{zz} = 0$$

A two-dimensional surface source distribution formulation is used to obtain this solution. When the body singularity strengths are determined, the perturbation velocities which they induce on the aerodynamic surfaces, or other regions of the field, are evaluated.

The assumptions of thin airfoil theory allow the effects of thickness and lift on aerodynamic surfaces to be considered independently. Therefore the effects of the aerodynamic surfaces can be simulated by source and vortex singularities accounting for the effects of thickness and lift respectively. The source and vortex distributions used in this program are in the form of quadrilateral panels having a constant source or vortex strength. The vortex panels have a system of trailing vorticies extending undeflected to downstream infinity. The use of a chordwise linearly varying source panel is provided as an option to eliminate singularities associated with sonic panel edges at supersonic Mach numbers. The panels are planar, that is they have no incidence to the free stream (although dihedral may be included), since thin airfoil theory allows the transfer of the singularities and boundary conditions to the plane of the mean chord. These boundary conditions are satisfied at a single control point on each panel. For thickness, the control point is located at the panel centroid while the effects of twist, camber, and angle of attack are satisfied at the spanwise centroid of each vortex panel and at 87.5 percent of its chord.

A cylindrical, non-circular, interference shell, composed entirely of vortex panels, is used to account for the interference effects of the aerodynamic surfaces on the fuselage and nacelles. The boundary conditions on an interference shell are such that the velocity normal to the shell induced by all singularities, except those of the body which it surrounds, is zero. The boundary conditions are satisfied at the usual control points for vortex panels.

The following sections define the details of the solution procedure. Included are discussions of the isolated body analysis, panel geometry, boundary conditions, and influence equations, the jet flap solution, and evaluation of aerodynamic characteristics including drag. References are cited for the reader interested in further pursuing a particular point.

Body Solution

According to slender body theory[1,2] the flow disturbance near a sufficiently regular three dimensional body may be represented by a perturbation potential of the form

$$\phi = \varphi(y,z;x) + g(x) \tag{1}$$

$\varphi(y,z;x)$ is a solution of the 2-D Laplace equation in the y, z cross flow plane satisfying the following boundary conditions

$$\nabla\varphi = jv + kw = 0$$

$$\frac{\partial \varphi}{\partial n} = 0 \qquad \text{on } C(x) \tag{2}$$

C(x) and n, are defined in figure 1 . A general solution for φ may be written as the real part of a complex potential function W(Z) with $Z = y + iz$.

$$\varphi = \mathrm{Re}\, W = \mathrm{Re}\left\{ A_0(x) \ln Z + \sum_{m=1}^{\infty} A_m(x) Z^{-m} \right\}$$

A useful alternative representation of φ and W is obtainable with the aid of Green's theorem[3]

$$\varphi = \mathrm{Re}\, W = -2\,\mathrm{Re} \oint_{c(x)} \sigma(\zeta) \ln(Z-\zeta)\, d\Delta \tag{3}$$

where $\sigma(\zeta)$ is a "source" density for values of $\zeta = y_c + iz_c$, (y_c, z_c) being coordinates of a point on the contour c(x).

The function g(x) is obtained by matching ϕ of equation (1) which is valid in the neighborhood of the body with an appropriate "outer" solution. g(x) is then found to depend explicitly on the Mach number M and longitudinal variation of cross sectional areas S(x)

$$g(x) = \frac{1}{2\pi}\left\{ S'(x)\ln(\tfrac{1}{2}\beta) - \tfrac{1}{2}\int_0^x S''(t)\ln(x-t)\,dt + \tfrac{1}{2}\int_x^1 S''(t)\ln(t-x)\,dt \right.$$
$$\left. - \tfrac{1}{2}S'(0)\ln x - \tfrac{1}{2}S'(1)\ln(1-x) \right\} \qquad M<1$$
$$g(x) = \frac{1}{2\pi}\left\{ S'(x)\ln(\tfrac{1}{2}\beta) - \int_0^x S''(t)\ln(x-t)\,dt \right\} \qquad M>1 \tag{4}$$

where

$$\beta = \sqrt{|1-M^2|}$$

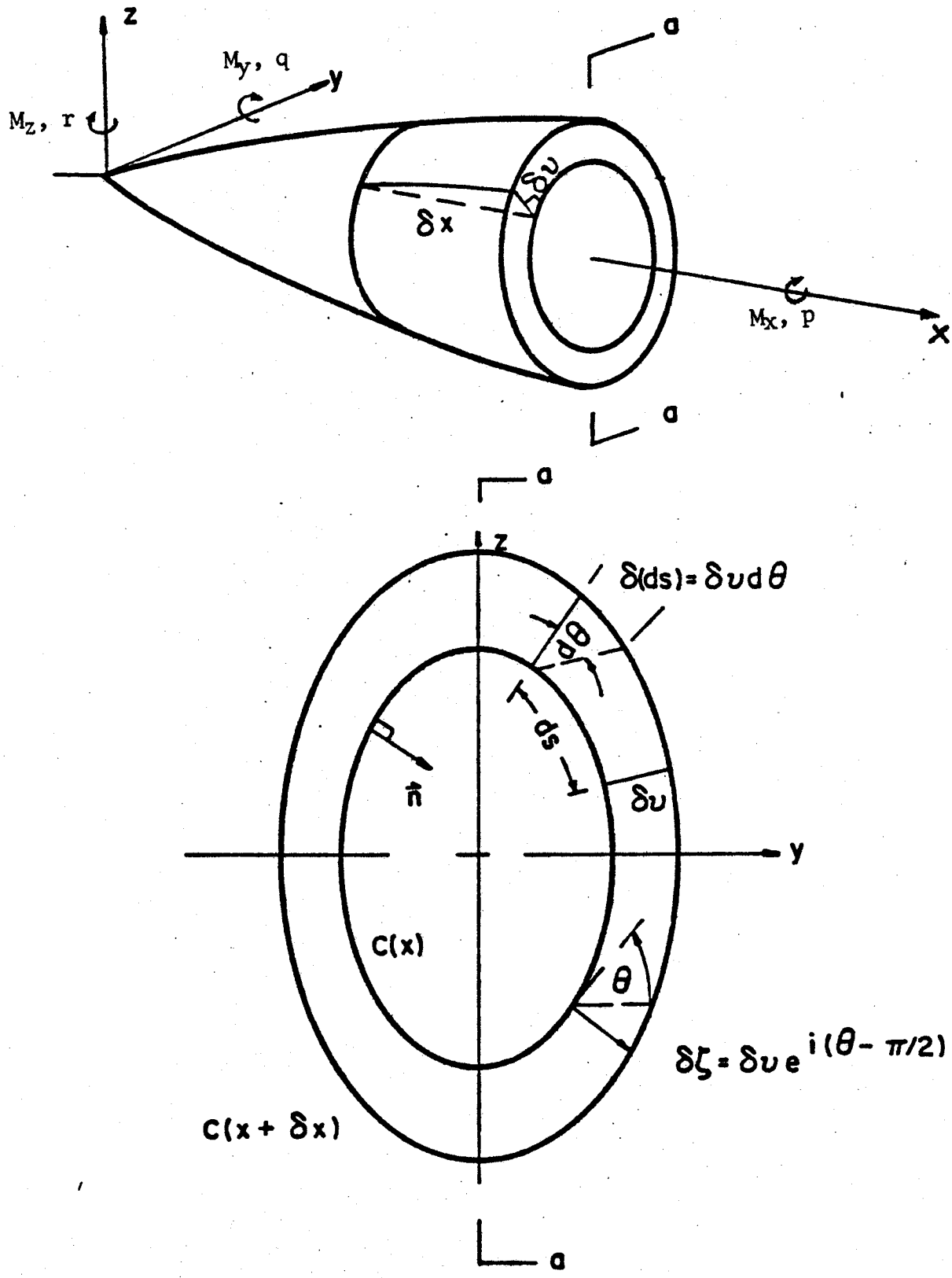

Figure 1. Body Slope and Crossectional Variables

The body axis perturbation velocities are obtained by differentiation of equation (1)

$$u = \phi_x = \phi_x + g'(x)$$

$$v = \phi_y$$

$$w = \phi_z$$

At supersonic speeds, zone of influence considerations require that $u = v = w = 0$ for $x - \beta r < 0$.

Solution of the preceding equations is based on an extension of the method of reference 4 .

Cross Flow Component

The reduction of computations to a numerical procedure utilizes the integral representation of ϕ given in equation (3) by discretization of the cross sectional boundary into a large number of short linear segments (figure 2) over each of which the source density σ is assumed constant at a value determined by boundary conditions.

Computation of $\sigma(i,n)$ over the segment i, i+1 proceeds by applying the boundary condition equation (2) at each segment of C_n. If $\nabla\phi = \vec{q} = \vec{j}v + \vec{k}w$ represents the velocity vector, the corresponding complex velocity in the cross flow plane is obtained by differentiation of W in equation (3) with respect to Z:

$$v - iw = -2\oint \frac{\sigma(\zeta)}{Z - \zeta}\, d\zeta \qquad (5)$$

The contribution by the sources located on segment i, i+1 to the velocity at $P_{j,n}$ is first evaluated. Noting that i, i+1 makes an angle $\theta(i,n)$ with respect to the horizontal axis, we have

$$d\zeta = d\zeta\, e^{i\theta(i,n)}$$

and the contribution to the integral in equation (5) may be written:

$$\Delta\left\{ v(j,n) \;\; iw(j,n) \right\} = -2\sigma(i,n)\, e^{-i\theta(i,n)} \int_{\zeta_{i,n}}^{\zeta_{i+1,n}} \frac{d\zeta}{Z_{j,n} - \zeta}$$

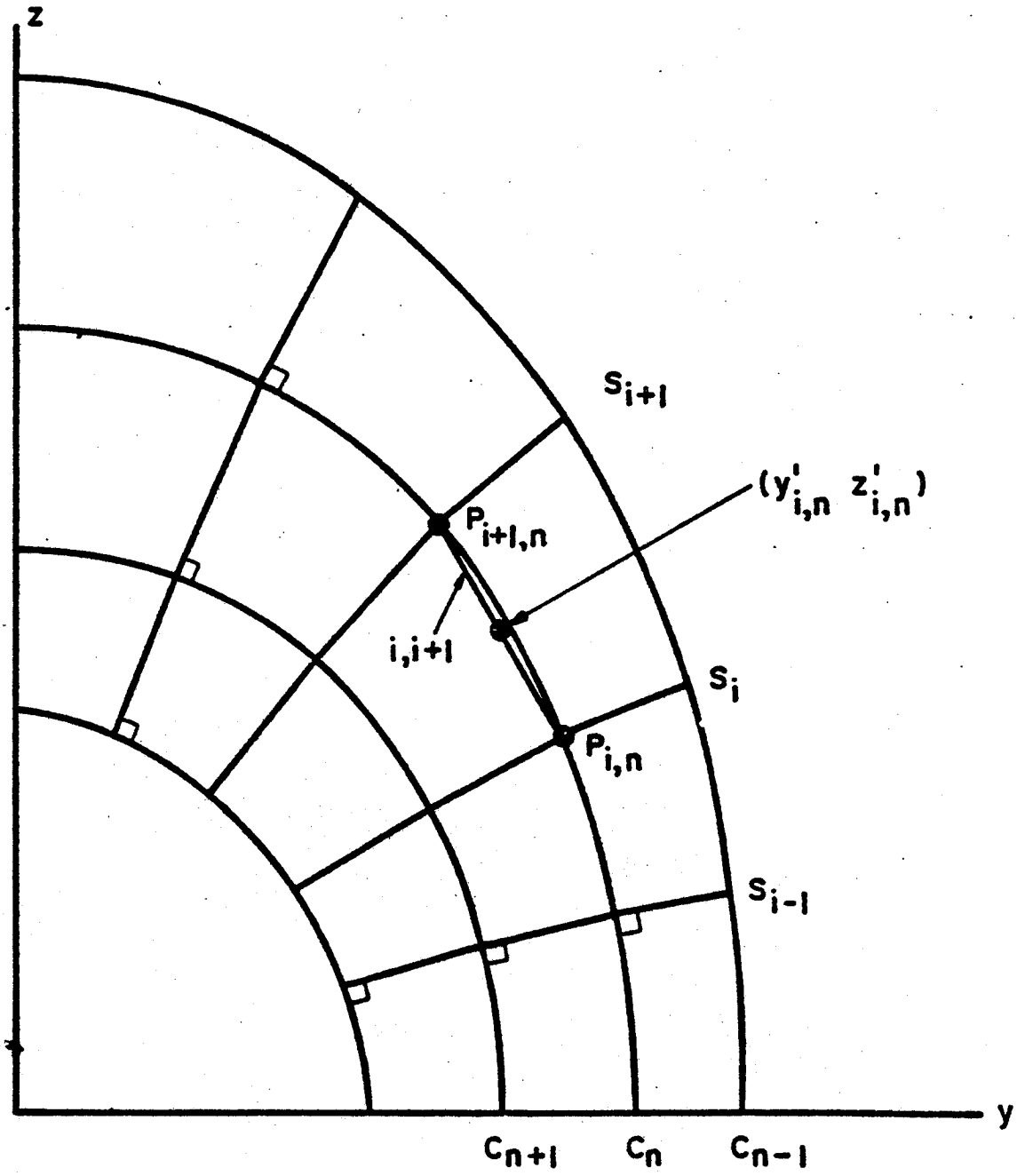

Figure 2. Crossection Boundary Segmenting Scheme

After integration of the last term and summation over all contributing segments, the result may be written

$$v(j,n) - i\,w(j,n) = -2\sum_{i} \sigma(i,n)\, e^{-i\theta(i,n)} \left\{ \ln \frac{R(i+1,j,n)}{R(i,j,n)} + i\,\delta(i,j,n) \right\} \qquad (6)$$

in which, referring to figure 3 , the quantities R(i,j,n) and $\delta(i,j,n)$ are defined by the relationships

$$R(i,j,n)\, e^{i\psi(i,j,n)} = Z'_{j,n} - Z_{i,n}$$

$$\delta(i,j,n) = \psi'(i,j,n) - \psi(i,j,n)$$

To insure uniqueness of the complex velocity, care must be exercised in assigning values to the angles $\psi(i,j,n)$ and $\psi'(i,j,n)$. Referring to figure 3 , these are measured counter-clockwise from the positive y axis so that when facing from $P_{i,n}$ to $P_{i+1,n}$, a point $P'_{j,n}$ just to the left of i,i+1 shall define an angle $\psi(i,j,n) = \theta(i,n)$. As $P'_{j,n}$ traverses a path around $P_{i,n}$ to a point just to the right of i,i+1, $\psi(i,j,n)$ increases from $\theta(i,n)$ to $\theta(i,n) + 2\pi$. The same holds true for $\psi'(i,j,n)$ as $P'_{j,n}$ traverses a path around $P_{i+1,n}$. In consequence of these definitions $\delta(i,j,n)$ becomes $-\pi$ when approaching i,i+1 from the right and π when approaching from the left. This discontinuity reflects that exhibited by the stream function upon traversing any closed path which encloses a distribution of finite sources.

From the boundary condition equation (2), we have

$$-\left(\frac{\partial \varphi}{\partial n}\right)_{j,n} = v(j,n) \sin\theta(j,n) - w(j,n) \cos\theta(j,n)$$

After substitution of v and w from equation (6), this last expression becomes

$$-\left(\frac{\partial \varphi}{\partial n}\right)_{j,n} = \sum_{i} a(j,i)\,\sigma(i,n) \qquad (7)$$

where

$$a(j,i) = 2\left\{ \sin[\theta(j,n) - \theta(i,n)] \ln \frac{R(i+1,j,n)}{R(i,j,n)} + \delta(i,j,n) \cos[\theta(j,n) - \theta(i,n)] \right\}$$

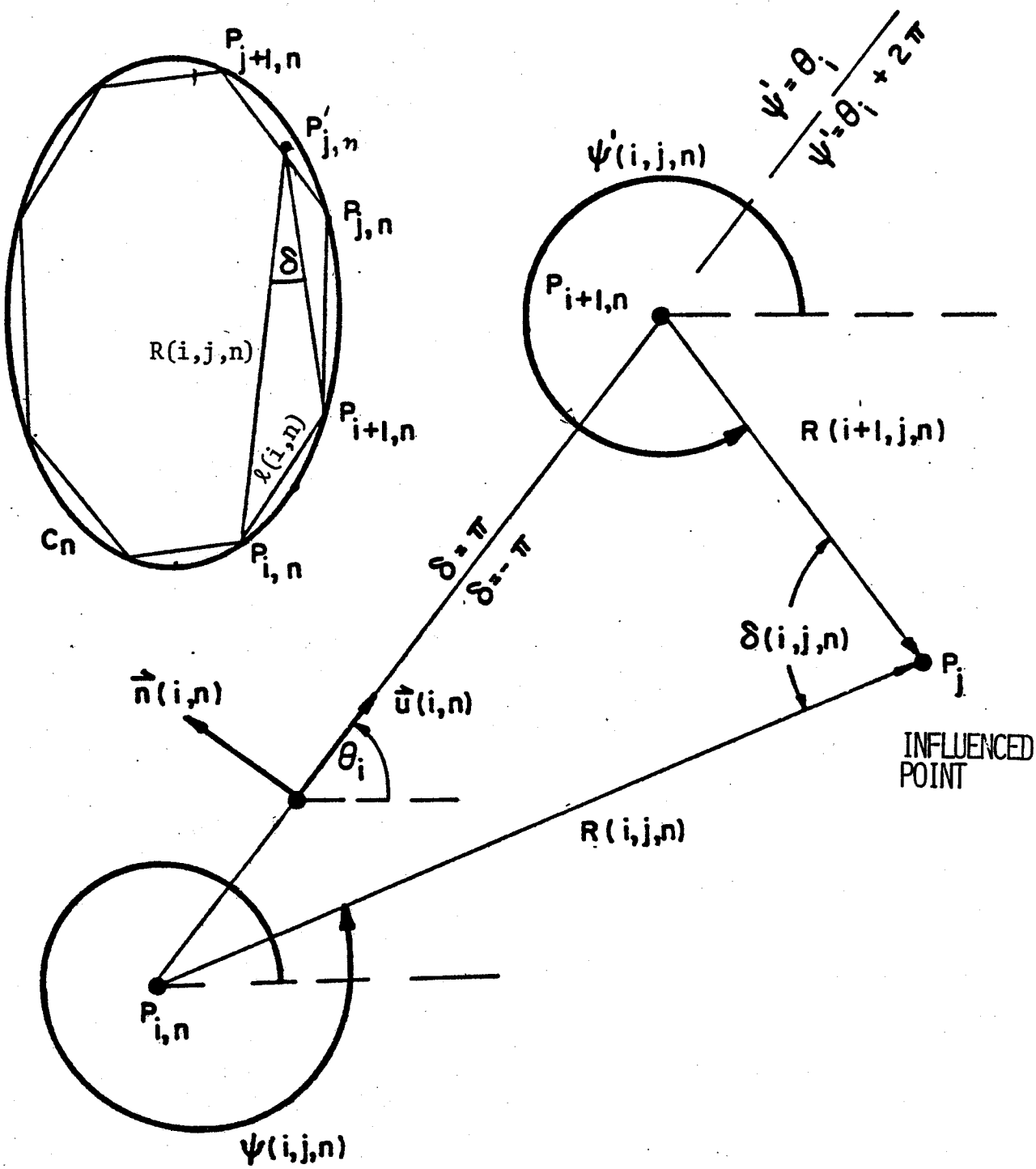

Figure 3. Details of Variables Pertaining to Segment i,i+1 of Boundary C_n

The surface normal perturbation velocity - $(\partial\varphi/\partial n)_{j,n}$ may be written in terms of the body slope $(\partial\nu/\partial x)_{j,n}$, the angles of attack α, and sideslip β and the angular velocities p,q,r as

$$-\left(\frac{\partial\varphi}{\partial n}\right)_{j,n} = \left(\frac{\partial\nu}{\partial x}\right)_{j,n} + \left[\alpha + \frac{1}{U}\, q(x-x_{cg}) + \frac{1}{U}\, py\right]\cos\theta(j,n)$$

$$+ \left[\beta - \frac{1}{U}\, r(x-x_{cg}) + \frac{p}{U}\,(z-z_{cg})\right]\sin\theta(j,n)$$

Satisfying equation 7 at each of the points $P'_{j,n}$ on a given contour boundary yields a set of equations for $\sigma(i,n)$.

Axisymmetric Component

Differentiation of g(x) must be carried out with due concern for the nature of the improper integrals appearing in equation (4). The result is

$$g'(x_m) = \frac{1}{4\pi}\left\{ S''(x_m)\ln\tfrac{1}{4}(1-M^2) + I_m(x_m) - J_m(x_m) \right.$$

$$\left. - \frac{1}{x_m}\, S'(0) + \frac{1}{(1-x_m)}\, S'(1) - S''(0)\ln x_m - S''(1)\ln(1-x_m)\right\} \qquad M<1$$

$$g'(x_m) = \frac{1}{2\pi}\left\{ \frac{1}{2}\, S''(x_m)\ln\tfrac{1}{4}(M^2-1) - J_m(x_m) - S''(0)\ln x_m \right\} \qquad M>1$$

where

$$I_m(x_m) = \int_{x_m}^{1} \ln(x_m - t)\, S'''(t)\, dt = \sum_{m=n}^{N-1} \left[S''_{m+1} - S''_m \right] \ln(x'_m - x_m)$$

$$J_m(x_m) = \int_{0}^{x_m} \ln(x_m - t)\, S'''(t)\, dt = \sum_{m=0}^{m-1} \left[S''_{m+1} - S''_m \right] \ln(x_m - x'_m)$$

$$x'_m = \tfrac{1}{2}(x_{m+1} + x_m)$$

To compute the second derivatives of the equivalent body cross sectional area required for g'(x), the first derivatives at x'_m are found by finite differences between x_m and x_{m+1}. Second derivatives $S''(x''_m)$ at x''_m $(x'_{m+1} + x'_m)/2$ are then found by finite differences between S' at x'_m and x'_{m+1}. Finally $S''(x_m)$ is determined by linear interpolation of $S''(x''_m)$ between x''_m and x''_{m+1}.

Perturbation Velocities

The axial velocity u depends on $(\partial\phi/\partial x)$ and the axisymmetric solution $g^*(x)$. $(\partial\phi/\partial x)$ is obtained by differentiation of the integral in equation (3) to first obtain an exact expression which is then approximated by evaluating the result over the segmented boundary.

The derivation of $\partial\phi/\partial x$ must take into account the fact that the path of integration in equation (3) is a function of x. Referring to figure 1 increments of a dependent variable taken along C(x) are denoted by $d(\ )$ and increments taken normal to C are denoted by $\delta(\ )$. Differentiation of equation (3) then yields

$$\frac{\partial\phi}{\partial x} = -2\,\mathrm{Re}\left\{ \oint \frac{\delta\sigma}{\delta x} \ln(Z-\zeta)\,ds - \oint \frac{\sigma(\zeta)}{Z-\zeta}\frac{\delta\zeta}{\delta x}\,ds + \oint \sigma(\zeta)\ln(Z-\zeta)\frac{\delta(ds)}{\delta x} \right\} \tag{8}$$

From figure 1

$$\delta(ds) = \delta\nu\, d\theta = \delta\nu \frac{ds}{h(\zeta)} \tag{9}$$

where $h(\zeta)$ is the radius of curvature of C(x) at ζ. In addition, we have from figure 1

$$\frac{\delta\zeta}{\delta x} = \frac{\delta\nu}{\delta x} e^{i(\theta-\frac{1}{2}\pi)} \tag{10}$$

To evaluate $\frac{\delta\sigma}{\delta x}$ we note,

$$\frac{\delta\sigma}{\delta x} = \lim_{\delta x \to 0} \frac{\sigma(i,n+1) - \sigma(i,n)}{\delta x} \tag{11}$$

Introducing equations (9), (10), and (11) into equation (8),

$$\frac{\partial\phi}{\partial x} = -2\,R_e \left\{ \oint \left[\left(\frac{\delta\sigma}{\delta x}\right)_o + \frac{\sigma}{h}\frac{\delta\nu}{\delta x} \right] \ln(z-\zeta)\,ds + i \oint \left[\sigma \frac{\delta\nu}{\delta x}\right] \frac{d\zeta}{z-\zeta} \right\}$$

Again, assuming that quantities in the brackets of the integrands are constant over i,i+1,

$$\left(\frac{\partial\phi}{\partial x}\right)_{j,n} = 2 \sum_i \left\{ \left[\left(\frac{\delta\sigma}{\delta x}\right)_o + \frac{\sigma}{h}\frac{\delta\nu}{\delta x} \right]_{i,n} \frac{\Delta\phi(i,j,n)}{\sigma(i,n)} - \sigma(i,n) \left(\frac{\delta\nu}{\delta x}\right)_{i,n} \delta(i,j,n) \right\}$$

where

$$\frac{\Delta\phi(i,j,n)}{\sigma(i,n)} = \left\{ \vec{R}(i+1,j,n) \cdot \vec{u}(i,n) \ln R(i+1,j,n) - \vec{R}(i,j,n) \cdot \vec{u}(i,n) \ln R(i,j,n) - \vec{R}(i,j,n) \cdot \vec{n}(i,n)\, \delta(i,j,n) + \ell(i,n) \right\}$$

The radius of curvature h(i,n) and the derivatives $\delta\sigma/\delta x$, $\delta\nu/\delta x$ are approximated at the mid points of the segments i,i+1 as follows

a) $\delta\sigma/\delta x$ - the derivative at the mid-point x'_n of the interval x_n, x_{n+1} is set equal to the divided difference between $\sigma(i,n)$ and $\sigma(i,n+1)$. Linear interpolation between these derivatives then yields $\delta\sigma/\delta x$ at x_n.

b) $\delta\nu/\delta x$ - referring to figure 4 , the displacement $\delta\eta$ is determined by linear interpolation between $\delta\zeta_{i,n}$ and $\delta\zeta_{i+1,n}$. $\delta\eta/(x_{n+1} - x_n)$ then represents $\delta\nu/\delta x$ at x'_n. Linear interpolation between the stations x'_n then yields $\delta\nu/\delta x$ at x_n.

c) 1/h: - θ at $P_{i,n}$ is determined by interpolation between values of $\theta(i,n)$ at $P'_{i,n}$. The curvature 1/h at $P'_{i,n}$ is then set equal to the divided difference between θ at $P_{i+1,n}$ and θ at $P_{i,n}$.

The lateral and vertical perturbation velocities, v and ω , are obtained from

$$v - i\omega = -2\oint \frac{\sigma(s)}{z-\zeta}\, ds$$

Integration over the boundary with constant segment source density yields:

$$v(j,n) - i\,\omega(j,n) = 2\sum_i \sigma(i,n)\, e^{i\theta(i,n)} \left\{ \ln \frac{R(i+1,j,n)}{R(i,j,n)} - i\,\delta(i,j,n) \right\}$$

Thus

$$v = \phi_y = 2\sum_i \sigma(i,n) \left\{ \ln \frac{R(i+1,j,n)}{R(i,j,n)} \cos\theta(i,n) - \delta(i,j,n) \sin\theta(i,n) \right\}$$

$$\omega = \phi_z = 2\sum_i \sigma(i,n) \left\{ \ln \frac{R(i+1,j,n)}{R(i,j,n)} \sin\theta(i,n) - \delta(i,j,n) \cos\theta(i,n) \right\}$$

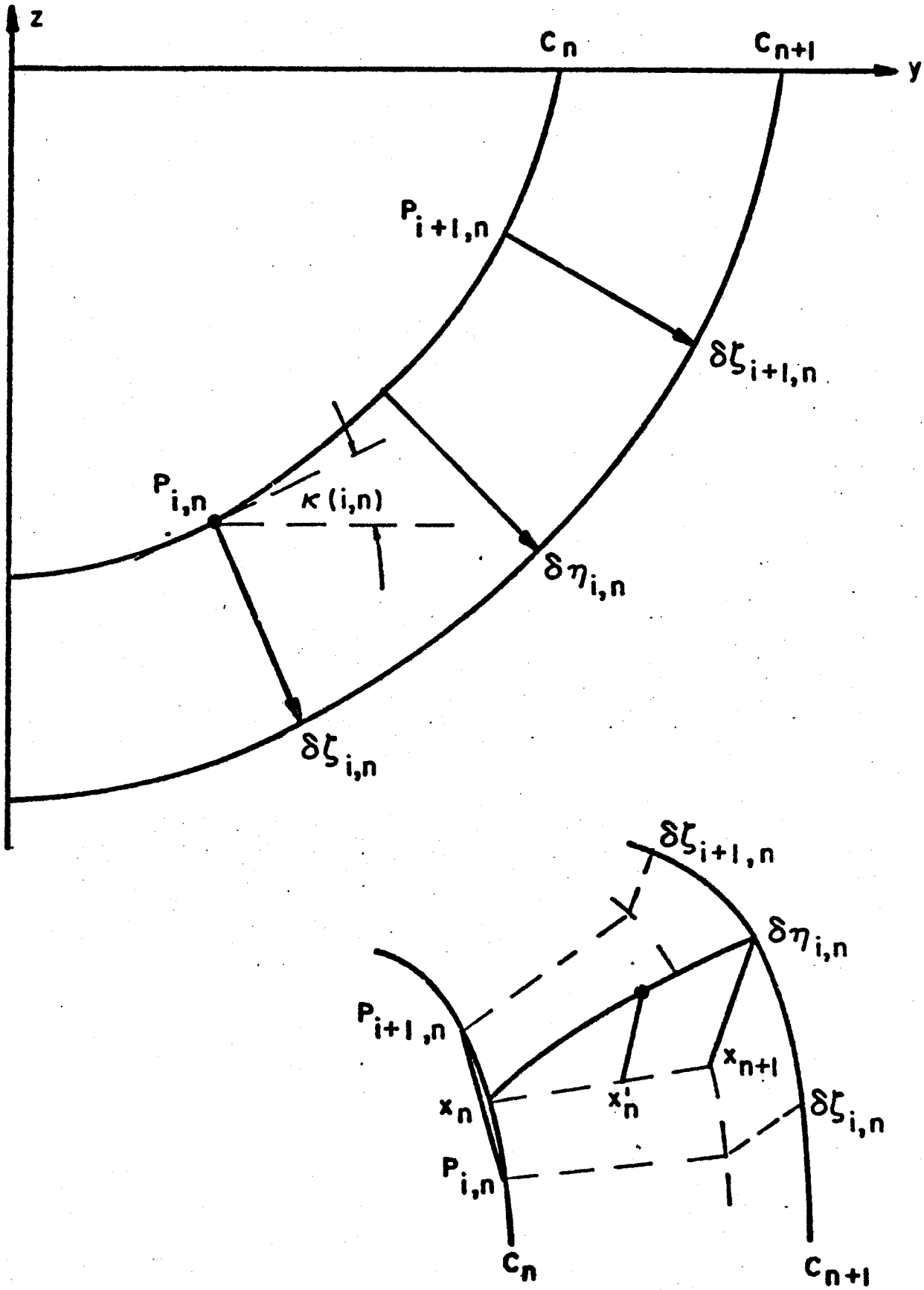

Figure 4. Interpolation Procedure for Determination of $(\delta\nu/\delta x)_{i,n}$

Panel Singularities

The source panels and vortex panels are composed of quadrilaterals with two edges parallel to the free stream. The coordinates of these panel corners are specified with respect to an (x,y,z) system having its x axis in the free stream direction and its z axis in the lift direction. However, the panel influence equations are written in terms of a coordinate system having a z axis normal to the panel and an x axis along one of the two parallel edges. A coordinate transformation is necessary to obtain the coordinates in the panel reference system. If the plane of the panel is inclined at an angle θ_p with respect to the y, z plane, a transformation into the panel coordinate system (x_p,y_p,z_p) is accomplished as follows:

$$x_p = x$$

$$y_p = y\cos\theta_p + z\sin\theta_p$$

$$z_p = -y\sin\theta_p + z\cos\theta_p$$

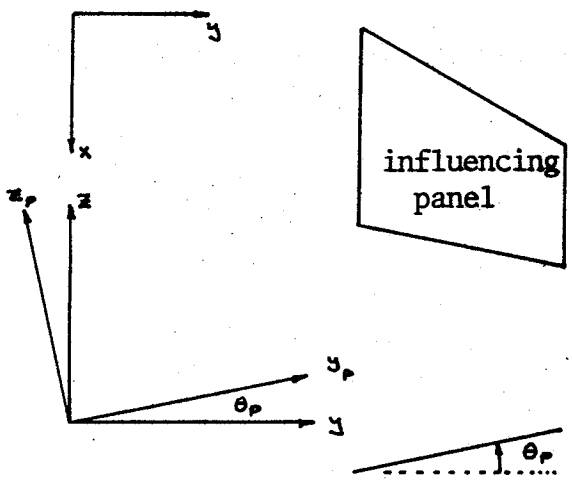

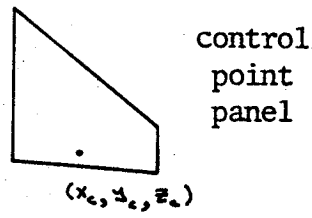

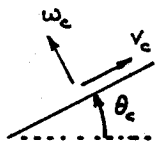

$$u_c = u_p$$

$$V_c = V_p\cos(\theta_c - \theta_p) + \omega_p\sin(\theta_p - \theta_c)$$

$$\omega_c = -V_p\sin(\theta_c - \theta_p) + \omega_p\cos(\theta_p - \theta_c)$$

A transformation of the (u_p,v_p,w_p) velocities into the coordinate system of the panel on which the control point is located (u_C,v_C,w_C) results in the axial, binormal and normal velocities induced on the panel.

For the image of the influencing panel, the signs of y, θ_C and v_C are changed while using the same calculation procedure.

Panel Singularity Strengths

The source singularity strengths may be found directly by equating each source panel strength to the slope of the thickness distribution at its control point. For panel i

$$\sigma_i = \left(\frac{dz_t}{dx}\right)_i$$

where Z_t refers to the shape of the thickness distribution. The influence equations for the source panels can then be used to obtain the velocities induced by the source panels anywhere in the flow.

The determination of the vortex panel singularity strengths are the final step in the solution procedure. They are obtained by solving a set of simultaneous equations utilizing the vortex panel influence equations to relate the singularity strengths to the boundary conditions at the control points of the vortex panels. The boundary conditions permit the condition of tangential flow to be satisfied.

Each vortex panel j having singularity strength C_{p_j} induces a set of velocities (A^{u}_{ij}, A^{v}_{ij}, A^{ω}_{ij}) on panel i. Therefore a set of influence equations can be written:

$$u_{c_i} = \sum_j A^{u}_{ij} C_{p_j} + u_{o_i}$$

$$v_{c_i} = \sum_j A^{v}_{ij} C_{p_j} + v_{o_i}$$

$$\omega_{c_i} = \sum_j A^{\omega}_{ij} C_{p_j} + \omega_{o_i}$$

where (u_{oi}, v_{oi}, w_{oj}) refer to the velocities induced by all other body and source singularities, and written in the coordinate system of the panel containing the control point. Since the resultant velocity along the normal at a panel control point must be zero,

$$\vec{U}\cdot\vec{n} = U\left[\vec{e}_x + u_c\vec{e}_x + v_c\vec{e}_b + \omega_c\vec{e}_n\right]\cdot\vec{n}$$

$$= U\left[(1+u_c)\vec{e}_x\cdot\vec{n} + \omega_c\right] = 0$$

$$(1+u_c)\vec{e}_x\cdot\vec{n} \approx -\left(\frac{dz_c}{dx}\right)_i$$

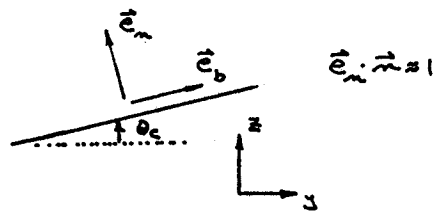

$\vec{e}_n\cdot\vec{n} = 1$

$$\omega_{c_i} = \left(\frac{dz_c}{dx}\right)_i$$

and the following system of equations results

$$\sum_j A^{\omega}_{ij} C_{p_j} = \left(\frac{dz_c}{dx}\right)_i - \omega_{o_i}$$

This set of linear equations can be solved for the C_{p_j} and, since it assumes symmetrical panel loading, can be used to determine the longitudinal characteristics. A similar set of equations exist for the calculation of the lateral/directional characteristics. This set assumes an antisymmetrical panel loading and has a correspondingly different set of influence coefficients A_{ij}.

Boundary Conditions

Several types of basic and unit boundary conditions are considered and can be classified as either symmetric or antisymmetric. Linearized theory allows the superposition of these basic unit solutions. The p, q and r rotary derivative boundary conditions are the result of placing the configuration at $\alpha = 0$, $\beta = 0$ in a flow field rotating at one radian per second.

Symmetric:

1) basic $(dz_c/dx) - \omega_{o_B} - \omega_{o_S}$

(dz_c/dx) = surface slope due to twist and camber

ω_{o_B} = normalwash induced by slender body thickness and camber

ω_{o_S} = normalwash induced by source panels

2) Unit alpha $-\frac{\pi}{180}\cos\theta_c - \omega_{\alpha_B}$

ω_{α_B} = normalwash induced by slender body at unit alpha

3) Unit q rotation $-\frac{2}{\bar{c}}(x - x_{cg})\cos\theta_c - \omega_{q_B}$

ω_{q_B} = normalwash induced by slender body undergoing unit q rotation

4) Unit flap $-\frac{\pi}{180}\sigma$

σ = 1. for flap panel

σ = 0. for others

Antisymmetric:

1) Unit beta $-\frac{\pi}{180}\sin\theta_c - \beta_B$

β_B = normalwash induced by slender body at unit sideslip

2) Unit p rotation $-\frac{2}{b}(y - y_{cg})\cos\theta_c - \frac{2}{b}(z - z_{cg}) - \omega_{p_B}$

ω_{p_B} = normalwash induced by slender body undergoing unit p rotation

3) Unit r rotation $\frac{2}{b}(x - x_{cg})\sin\theta_c - \omega_{r_B}$

ω_{r_B} = Normalwash induced by slender body undergoing unit r rotation

4) Unit flap $\frac{\pi}{180}\sigma$

σ = 1. for flap panel

σ = 0. for others

Constant Source and Constant Vorticity Panel Influence Equations

A constant pressure or constant source panel with a quadrilateral shape can be constructed by adding or subtracting four semi-infinite triangular shaped panels[5]. These semi-infinite triangles, each determined by a corner of the quadrilateral, can be assumed to induce a velocity perturbation everywhere in the flow. However, each corner represents only an integration limit, and all four corners must be included to make any sense.

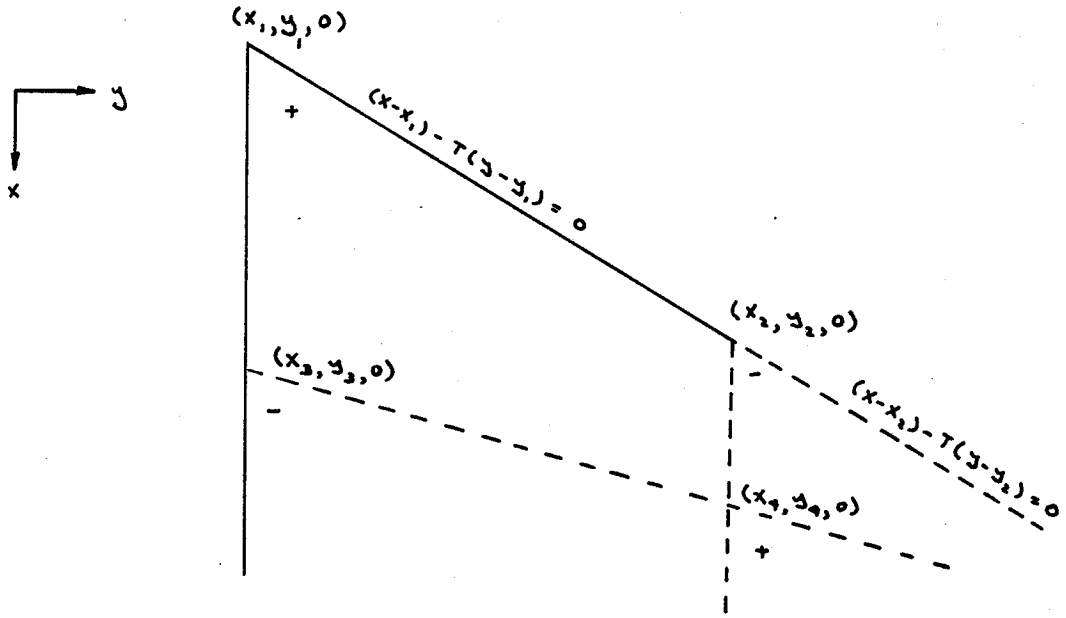

If it is kept in mind that four corners must be included, one of these triangles having sides determined by $y = 0$ and $x-Ty = 0$, induces the following perturbation velocities:

$$k = \begin{cases} 1 & \beta^2 > 0 \\ 2 & \beta^2 < 0 \end{cases}$$

$$\beta^2 = 1 - M^2$$

$$R^2 = x^2 + \beta^2(y^2 + z^2)$$

Constant source panel

$$u(x,y,z,T) = -\frac{k\sigma}{2\pi}\frac{1}{\sqrt{T^2+\beta^2}}\frac{1}{2}\log\frac{\sqrt{T^2+\beta^2}\,R + (Tx+\beta^2 y)}{\sqrt{T^2+\beta^2}\,R - (Tx+\beta^2 y)}$$

$$v(x,y,z,T) = -\frac{k\sigma}{2\pi}\left\{\frac{1}{2}\log\frac{R+x}{R-x} - \frac{T}{\sqrt{T^2+\beta^2}}\frac{1}{2}\log\frac{\sqrt{T^2+\beta^2}\,R + (Tx+\beta^2 y)}{\sqrt{T^2+\beta^2}\,R - (Tx+\beta^2 y)}\right\}$$

$$w(x,y,z,T) = -\frac{k\sigma}{2\pi}\tan^{-1}\frac{zR}{xy - T(y^2+z^2)}$$

Constant vorticity panel

$$u(x,y,z,T) = \frac{kc_p}{8\pi}\left\{\tan^{-1}\frac{zR}{xy-T(y^2+z^2)} - (2-k)\tan^{-1}\frac{y}{z}\right\}$$

$$v(x,y,z,T) = -\frac{kc_p}{8\pi}\left\{T\tan^{-1}\frac{zR}{xy-T(y^2+z^2)} + \frac{zR}{y^2+z^2} - (2-k)\left[T\tan^{-1}\frac{y}{z} - \frac{zx}{y^2+z^2}\right]\right\}$$

$$w(x,y,z,T) = \frac{kc_p}{8\pi}\left\{T\frac{1}{2}\log\frac{R+x}{R-x} - \sqrt{T^2+\beta^2}\,\frac{1}{2}\log\frac{\sqrt{T^2+\beta^2}\,R + (Tx+\beta^2 y)}{\sqrt{T^2+\beta^2}\,R - (Tx+\beta^2 y)} + \frac{yR}{y^2+z^2}\right.$$

$$\left. + (2-k)\left[\frac{xy}{y^2+z^2} - T\frac{1}{2}\log(y^2+z^2)\right]\right\}$$

These perturbation velocities hold for both supersonic and subsonic free stream velocities. In supersonic flow only the real and downstream contributions are considered.

To establish that these are the correct perturbation velocities the following criteria must be met:

1. Laplace's equation must be satisfied

$$\beta^2 \Phi_{xx} + \Phi_{yy} + \Phi_{zz} = 0$$

or the equivalent,

$$u_y = v_x$$

$$u_z = \omega_x$$

$$v_z = \omega_y$$

$$\beta^2 u_x + v_y + \omega_z = 0$$

2. The correct discontinuity or jump in the perturbation velocity must occur at the surface of the quadrilateral panel area. For the source panel the jump occurs in the normal or w velocity and on the vortex panel there must be a jump of constant magnitude in the u perturbation velocity over the panel area. The perturbation velocities should be continuous elsewhere, except on the trailing vortex sheet of the vortex panel.

3. The perturbation velocities must go to zero as upstream infinity is approached.

4. For the vortex panel the trailing vorticity must extend straight back to downstream infinity. This means that any discontinuity in the v velocity must be zero outside the spanwise boundaries of the panel and must be zero upstream of the panel.

The first criteria can be established by using the derivatives given in TABLE I.

The second criteria can be established by noting that all terms except

$$\tan^{-1}\frac{zR}{xy - T(y^2+z^2)} \quad \text{and} \quad \tan^{-1}\frac{y}{z}$$

are continuous at Z = 0. Consider these terms keeping in mind that the contributions from all four corners must included.

If we let

$$\xi = (x-x_1) - T(y-y_1) = (x-x_2) - T(y-y_2)$$

$$R_i^2 = (x-x_i)^2 + \beta^2[(y-y_i)^2 + z^2]$$

and use

$$\tan^{-1} A + \tan^{-1} B = \tan^{-1}\frac{A+B}{1-AB}$$

then the contributions from both corners on the leading edge can be combined as follows.

$$\tan^{-1}\frac{zR_1}{\xi(y-y_1) - Tz^2} - \tan^{-1}\frac{zR_2}{\xi(y-y_2) - Tz^2}$$

$$= \tan^{-1}\left\{ z\,\frac{[\xi(y-y_2) - Tz^2]R_1 - [\xi(y-y_1) - Tz^2]R_2}{[\xi(y-y_2) - Tz^2][\xi(y-y_1) - Tz^2] + z^2R_1R_2} \right\}$$

TABLE I

DERIVATIVES

$$R^2 = x^2 + \beta^2(y^2+z^2)$$

$$R\frac{\partial}{\partial x}R = x$$

$$\frac{\partial}{\partial x}\ \frac{1}{2}\log\frac{R+x}{R-x} = \frac{1}{R}$$

$$\frac{\partial}{\partial x}\ \frac{1}{\sqrt{T^2+\beta^2}}\ \frac{1}{2}\log\frac{\sqrt{T^2+\beta^2}\,R+(Tx+\beta^2 y)}{\sqrt{T^2+\beta^2}\,R-(Tx+\beta^2 y)} = -\frac{xy-T(y^2+z^2)}{\left[(x-Ty)^2+(\beta^2+T^2)z^2\right]}\ \frac{1}{R}$$

$$\frac{\partial}{\partial x}\ \tan^{-1}\frac{zR}{xy-T(y^2+z^2)} = -\frac{z(Tx+\beta^2 y)}{\left[(x-Ty)^2+(\beta^2+T^2)z^2\right]}\ \frac{1}{R}$$

$$R\frac{\partial}{\partial y}R = \beta^2 y$$

$$\frac{\partial}{\partial y}\ \frac{1}{2}\log\frac{R+x}{R-x} = -\frac{xy}{(y^2+z^2)}\ \frac{1}{R}$$

$$\frac{\partial}{\partial y}\ \frac{1}{\sqrt{T^2+\beta^2}}\ \frac{1}{2}\log\frac{\sqrt{T^2+\beta^2}\,R+(Tx+\beta^2 y)}{\sqrt{T^2+\beta^2}\,R-(Tx+\beta^2 y)} = \frac{\left[x(x-Ty)+\beta^2 z^2\right]}{(x-Ty)^2+(\beta^2+T^2)z^2}\ \frac{1}{R}$$

$$\frac{\partial}{\partial y}\ \tan^{-1}\frac{zR}{xy-T(y^2+z^2)} = -\frac{xz}{y^2+z^2}\frac{1}{R}+\frac{Tz(Tx+\beta^2 y)}{(x-Ty)^2+(\beta^2+T^2)z^2}\ \frac{1}{R}$$

$$R\frac{\partial}{\partial z}R = \beta^2 z$$

$$\frac{\partial}{\partial z}\ \frac{1}{2}\log\frac{R+x}{R-x} = -\frac{xz}{y^2+z^2}\ \frac{1}{R}$$

$$\frac{\partial}{\partial z}\ \frac{1}{\sqrt{T^2+\beta^2}}\ \frac{1}{2}\log\frac{\sqrt{T^2+\beta^2}\,R+(Tx+\beta^2 y)}{\sqrt{T^2+\beta^2}\,R-(Tx+\beta^2 y)} = -\frac{z(Tx+\beta^2 y)}{(x-Ty)^2+(\beta^2+T^2)z^2}\ \frac{1}{R}$$

$$\frac{\partial}{\partial z}\ \tan^{-1}\frac{zR}{xy-T(y^2+z^2)} = \frac{xy}{y^2+z^2}\frac{1}{R}+\frac{(x-Ty)(Tx+\beta^2 y)}{(x-Ty)^2+(\beta^2+T^2)z^2}\ \frac{1}{R}$$

If we define

$$\Delta \operatorname{sgn} z = \begin{cases} 1 & z > 0 \\ -1 & z < 0 \end{cases}$$

$$\lim_{a \to 0} \tan^{-1} \frac{a}{b} = \begin{cases} 0 & b > 0 \\ \pi \operatorname{sgn} a & b < 0 \end{cases} \qquad -\pi \le \tan^{-1} c \le \pi$$

$$\Delta f(z) = \lim_{z \to 0^+} f(z) - \lim_{z \to 0^-} f(z)$$

then

$$\lim_{z \to 0} \left\{ \tan^{-1} \frac{z R_1}{\xi (y - y_1) - \tau z^2} - \tan^{-1} \frac{z R_2}{\xi (y - y_2) - \tau z^2} \right\} = \begin{cases} 0 & (y-y_1)(y-y_2) > 0 \\ -\pi \operatorname{sgn} z \operatorname{sgn} \xi & (y-y_1)(y-y_2) < 0 \end{cases}$$

$$\Delta \left\{ \tan^{-1} \frac{z R_1}{\xi (y - y_1) - \tau z^2} - \tan^{-1} \frac{z R_2}{\xi (y - y_2) - \tau z^2} \right\} = \begin{cases} 0 & (y-y_1)(y-y_2) > 0 \\ -2\pi \operatorname{sgn} \xi & (y-y_1)(y-y_2) < 0 \end{cases}$$

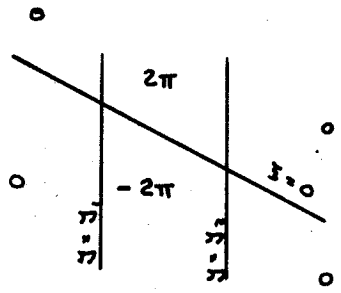

Therefore when a similar procedure is carried out for the trailing edge of a source panel we obtain the following jump in the w perturbation velocity.

$$\Delta \omega = 0$$

For the vortex panel (subsonic) we have an additional term. Considering both additional terms from the leading edge corners:

$$\tan^{-1}\frac{(y-y_1)}{z}-\tan^{-1}\frac{y-y_2}{z}=\tan^{-1}\frac{z(y_2-y_1)}{(y-y_1)(y-y_2)+z^2}$$

$$\lim_{z\to 0}\left\{\tan^{-1}\frac{(y-y_1)}{z}-\tan^{-1}\frac{y-y_2}{z}\right\}=\begin{cases}0 & (y-y_1)(y-y_2)>0\\ \pi\,\mathrm{sgn}\,z & (y-y_1)(y-y_2)<0\end{cases}$$

$$\Delta\left\{\tan^{-1}\frac{y-y_1}{z}-\tan^{-1}\frac{y-y_2}{z}\right\}=\begin{cases}0 & (y-y_1)(y-y_2)>0\\ 2\pi & (y-y_1)(y-y_2)<0\end{cases}$$

Therefore combining the terms

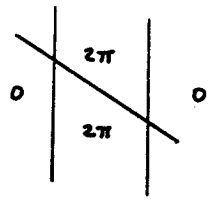

$$\Delta\left\{\tan^{-1}\frac{zR_1}{\xi(y-y_1)-Tz^2}-\tan^{-1}\frac{zR_2}{\xi(y-y_2)-Tz^2}-\tan^{-1}\frac{(y-y_1)}{z}+\tan^{-1}\frac{(y-y_2)}{z}\right\}$$

$$=\begin{cases}0 & (y-y_1)(y-y_2)>0\\ & \xi<0\\ -4\pi & \text{otherwise}\end{cases}$$

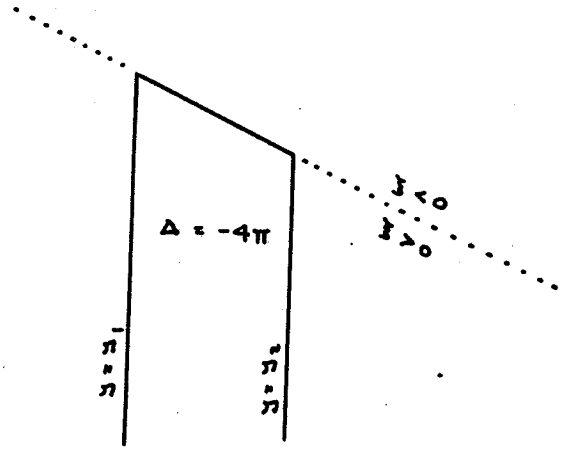

The contribution from each panel corner is:

$$\Delta u = \frac{C_p}{8\pi} \Delta \left\{ \tan^{-1} \frac{zR}{xy - T(y^2+z^2)} - \tan^{-1} \frac{y}{z} \right\}$$

$$\Delta V = -\frac{C_p T}{8\pi} \Delta \left\{ \tan^{-1} \frac{zR}{xy - T(y^2+z^2)} - \tan^{-1} \frac{y}{z} \right\}$$

Therefore summing all four panel corners

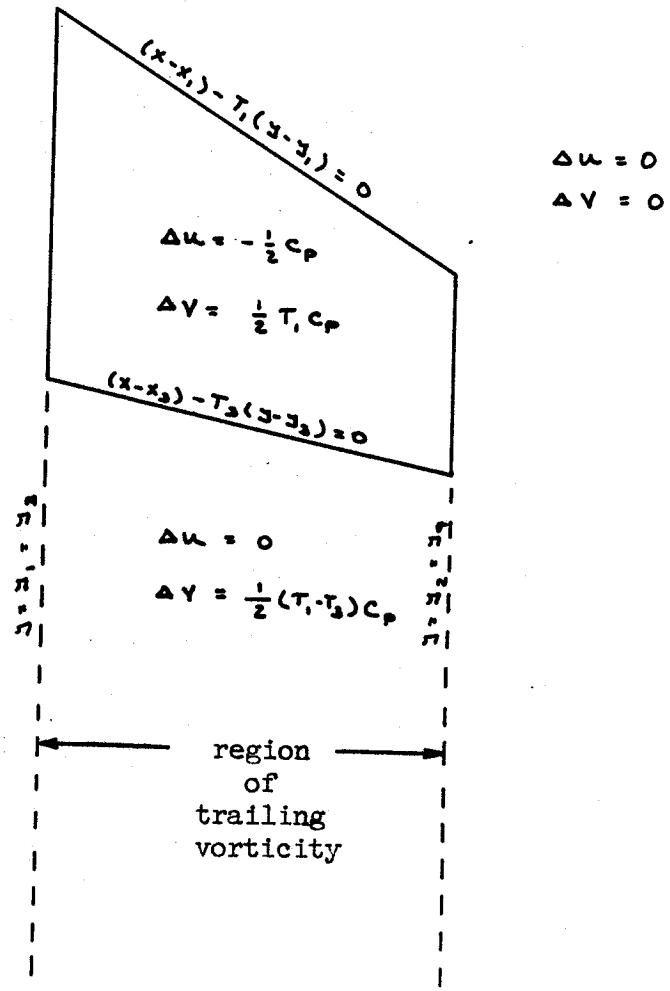

To verify the third criteria we must show that all of the functions approach zero when all four corners are considered as $x \to -\infty$

$$\frac{1}{2}\log\frac{R+x}{R-x} - \frac{1}{2}\log(y^2+z^2)$$

$$= \frac{1}{2}\log\frac{\beta^2(y^2+z^2)}{(R-x)^2} - \frac{1}{2}\log(y^2+z^2)$$

$$= -\frac{1}{2}\log(R-x)^2 + \frac{1}{2}\log\beta^2$$

Therefore considering both corners on the leading edge of the panel

$$\lim_{x\to-\infty} R = |x|$$

$$\lim_{x\to-\infty}\left\{\frac{1}{2}\log\frac{R_1+(x-x_1)}{R_1+(x-x_1)} - \frac{1}{2}\log\frac{R_2+(x-x_2)}{R_2-(x-x_2)}\right\} = \lim_{x\to-\infty}\frac{1}{2}\log\frac{(x-x_2)^2}{(x-x_1)^2} = 0$$

$$\lim_{x\to-\infty}\frac{R_1+(x-x_1)}{(y-y_1)^2+z^2} = 0$$

$$\lim_{x\to-\infty}\frac{1}{2}\log\frac{\sqrt{T^2+\beta^2}\,R+(Tx+\beta^2 y)}{\sqrt{T^2+\beta^2}\,R-(Tx+\beta^2 y)} = \frac{1}{2}\log\frac{\sqrt{T^2+\beta^2}-T}{\sqrt{T^2+\beta^2}+T}$$

and therefore this limit is also zero when both corners of the leading or trailing edges are considered. Since all terms are accounted for, the perturbation velocities are zero far upstream.

Since

$$(T^2+\beta^2)R^2 - (Tx+\beta^2 y)^2 = \beta^2\left[(x-Ty)^2 + (T^2+\beta^2)z^2\right]$$

$$\frac{1}{2}\log\frac{\sqrt{T^2+\beta^2}\,R + (Tx+\beta^2 y)}{\sqrt{T^2+\beta^2}\,R - (Tx+\beta^2 y)} = \frac{1}{2}\log\frac{\left[\sqrt{T^2+\beta^2}\,R + (Tx+\beta^2 y)\right]^2}{\beta^2\left[(x-Ty)^2+(T^2+\beta^2)z^2\right]}$$

$$= -\frac{1}{2}\log\frac{\beta^2\left[(x-Ty)^2+(T^2+\beta^2)z^2\right]}{\left[\sqrt{T^2+\beta^2}\,R - (Tx+\beta^2 y)\right]^2}$$

there is an apparent singularity along the line

$$(x-Ty) = 0 \quad , \quad z = 0$$

However this singularity may be removed by combining the contributions from both corners of the leading or trailing edges of the panel. Along either of these edges the values of

$$(x-x_i) - T(y-y_i) \quad \text{and} \quad z$$

are the same for each of the panel corners.

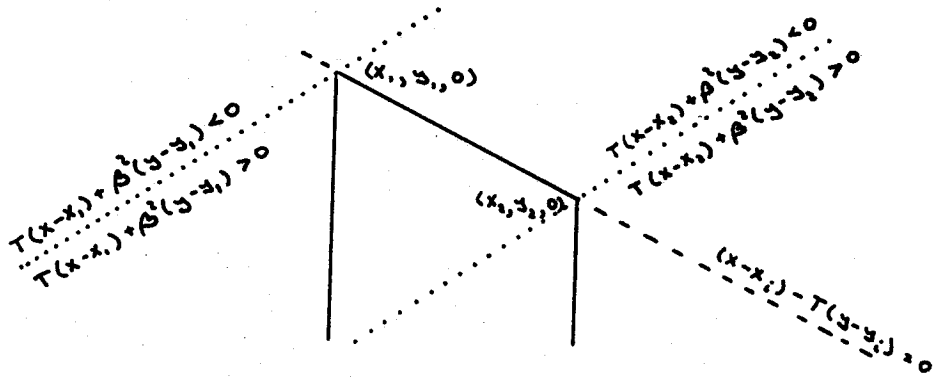

It can be seen from the above diagram that $(Tx+\beta^2 y)$ will have the same sign on a point (x,y,o) which lies outside the spanwise boundaries of the quadrilateral. Therefore outside the spanwise boundaries the term

$$\log\left[(x-Ty)^2 + (T^2+\beta^2)z^2\right]$$

can be canceled by combining both corners, and the resulting term

$$\pm\frac{1}{2}\log\frac{\sqrt{T^2+\beta^2}\;R_1 \pm \left[T(x-x_1)+\beta^2(y-y_1)\right]}{\sqrt{T^2+\beta^2}\;R_2 \pm \left[T(x-x_2)+\beta^2(y-y_1)\right]}$$

will not be singular if the correct + or - sign is chosen. Within the spanwise boundary an actual singularity occurs on the panel edge.

The term $\frac{1}{2}\log\frac{R+x}{R-x}$ also has a possible singularity. This term can be written

$$\frac{1}{2}\log\frac{R+x}{R-x} = \frac{1}{2}\log\frac{(R+x)^2}{\beta^2(y^2+z^2)}$$

For the source panel the singularity may be removed for points along $y^2+z^2=0$ which are outside of the panel boundaires.

If $(x-x_1)$ and $(x-x_3)$ have the same sign the combination of the two terms gives

$$\frac{1}{2}\log\frac{R_1+(x-x_1)}{R_1-(x-x_1)} - \frac{1}{2}\log\frac{R_2+(x-x_2)}{R_2-(x-x_2)} = \pm\frac{1}{2}\log\frac{R_1\pm(x-x_1)}{R_3\pm(x-x_3)}$$

where the correct sign is chosen to remove the singularity. On the panel edge the singularity is real and cannot be removed.

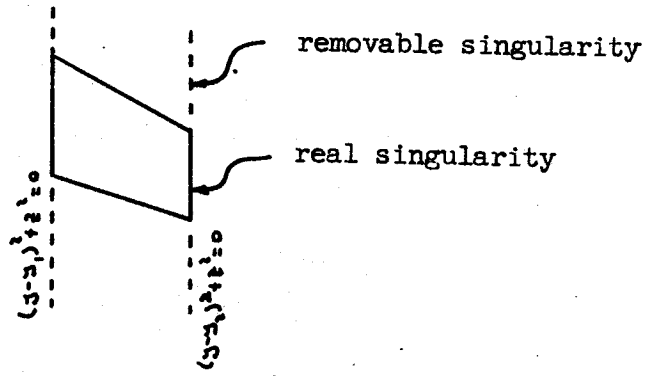

For a vortex panel the terms (subsonic)

$$\frac{1}{2}\log\frac{R+x}{R-x} - \frac{1}{2}\log(y^2+z^2) \quad \text{and} \quad \frac{y(R+x)}{(y^2+z^2)}$$

Both have real singularities for $x>0$ (downstream) and removable singularities for $x<0$ (upstream). The real singularities occur on the panel edges and on the edge of the trailing vortex sheet.

$$\text{if} \quad x<0 \qquad \lim_{(y^2+z^2)\to 0}\frac{y(R+x)}{y^2+z^2} = -\frac{1}{2}\beta^2\frac{y}{x}$$

Supersonic Velocities - Special Considerations

The velocity perturbation influence equations for supersonic flows are treated by taking only the real parts of the expressions. This means that $R = \sqrt{x^2-\beta^2(y^2+z^2)}$ is set equal to zero for points which lie outside the downstream mach cone from any given corner. Therefore R and $\frac{1}{2}\log\frac{R+x}{R-x}$ are zero for points which lie outside the downstream Mach cone. For $(\tau^2-\beta^2)>0$ there are no problems using this method.

If $(\tau^2-\beta^2)<0$ the real part of $\dfrac{1}{\sqrt{\tau^2-\beta^2}}\,\dfrac{1}{2}\log\dfrac{(\tau x-\beta^2 y)+\sqrt{\tau^2-\beta^2}\,R}{(\tau x-\beta^2 y)-\sqrt{\tau^2-\beta^2}\,R}$

is $\dfrac{1}{\sqrt{\beta^2-\tau^2}}\tan^{-1}\dfrac{\sqrt{\beta^2-\tau^2}\,R}{(\tau x-\beta^2 y)}$

therefore combining two corners

$$F2 = \frac{1}{\sqrt{\beta^2-\tau^2}}\tan^{-1}\frac{\sqrt{\beta^2-\tau^2}\left\{[\tau(x-x_2)-\beta^2(y-y_0)]R_1-[\tau(x-x_1)-\beta^2(y-y_0)]R_2\right\}}{[\tau(x-x_2)-\beta^2(y-y_0)][\tau(x-x_1)-\beta^2(y-y_0)]+(\beta^2-\tau^2)R_1R_2}$$

If $z = 0$ and either R_1 or R_2 is zero and we allow the other to approach zero the value of F2 becomes

$$F2 = \begin{cases} \dfrac{\pi}{\sqrt{\beta^2-\tau^2}} & [\tau(x-x_1)-\beta^2(y-y_0)][\tau(x-x_2)-\beta^2(y-y_0)] < 0 \\ 0 & [\tau(x-x_1)-\beta^2(y-y_0)][\tau(x-x_2)-\beta^2(y-y_0)] > 0 \end{cases}$$

Therefore if R_1 and R_2 are zero but we are inside the envelope of mach cones from the leading edge (see figure 5) the value of F2 is set equal to

$$F2 = \frac{\pi}{\sqrt{\beta^2-\tau^2}}$$

$$\text{if} \quad \begin{cases} [\tau(x-x_1)-\beta^2(y-y_0)][\tau(x-x_2)-\beta^2(y-y_0)] < 0 \\ R_1^2 < 0 \qquad R_2^2 < 0 \\ (x-\tau y)^2 > (\beta^2-\tau^2)z^2 \end{cases}$$

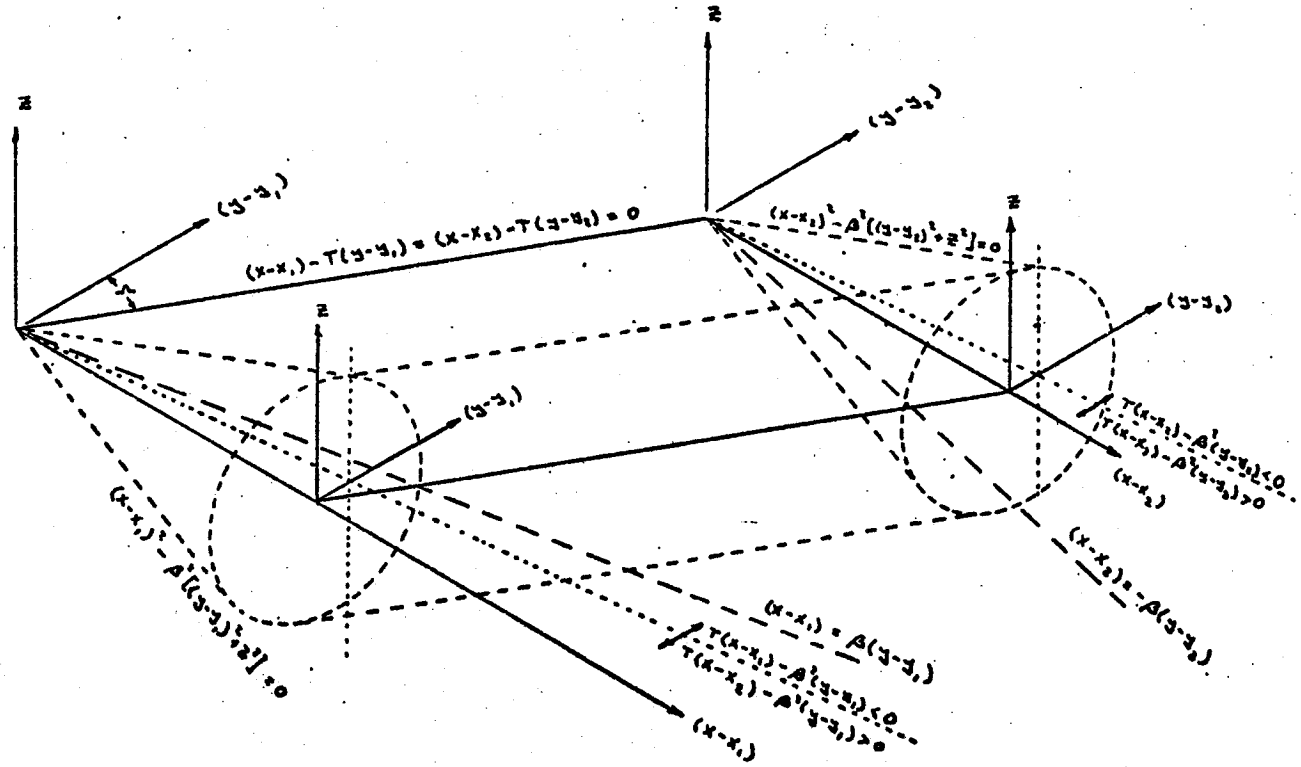

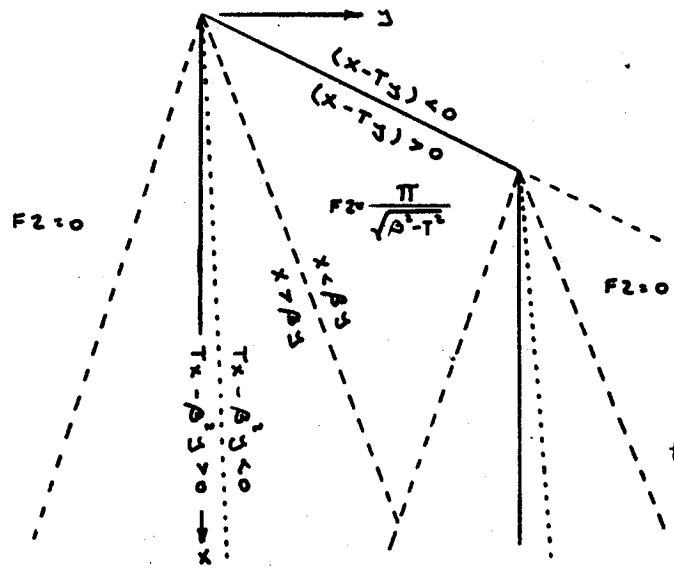

intersection of $(x-Ty)^2 = (\beta^2 - T^2) z^2$

and $x^2 = \beta^2(y^2 + z^2)$

occurs on the line $\begin{cases} y = ax \\ z = bx \end{cases}$

therefore $1 = \beta^2(a^2 + b^2)$

$1 - 2aT + T^2a^2 = (\beta^2 - T^2)b^2$

$\beta^2(1 - 2aT + T^2a^2) = (1 - \beta^2a^2)(\beta^2 - T^2) = \beta^2(\beta^2 - T^2)b^2$

$\beta^4a^2 - 2\beta^2Ta + T^2 = 0 \qquad \beta^2a = T$

$\beta^4b^2 = \beta^2 - T^2 \qquad \beta^2b = \pm\sqrt{\beta^2 - T^2}$

therefore the line is determined by

$Tx - \beta^2 y = 0 \qquad \beta^2 z^2 = (\beta^2 - T^2)x^2$

or $Tx - \beta^2 y = 0 \qquad (x-Ty)^2 = (\beta^2 - T^2) z^2$

Figure 5 Supersonic Leading Edge Mach Cone Envelope

As $T \to \beta$ (sonic leading edge) the value of $(T^2 - \beta^2) \to 0$. In this case

$$\lim_{T \to \beta} F2 = \frac{(R_1 - R_2)}{T\left[(x - x_1) - T(y - y_1)\right]} \qquad \left[(x - x_1) - T(y - y_1)\right] > 0$$

Linearly Varying Source Panel Influence Equations

In supersonic flow constant source panels having a sonic edge have a real singularity along an extension of this edge. The singularity occurs because:

$$\lim_{\substack{(x-x_1)\to T(y-y_1) \\ \epsilon^2=(T^2+\beta^2)\to 0}} \frac{1}{\epsilon}\left\{\frac{1}{2}\log\frac{\epsilon R_1+[T(x-x_1)+\beta^2(y-y_1)]}{\epsilon R_1-[T(x-x_1)+\beta^2(y-y_1)]}-\frac{1}{2}\log\frac{\epsilon R_2+[T(x-x_2)+\beta^2(y-y_2)]}{\epsilon R_2-[T(x-x_2)+\beta^2(y-y_2)]}\right\}=\infty$$

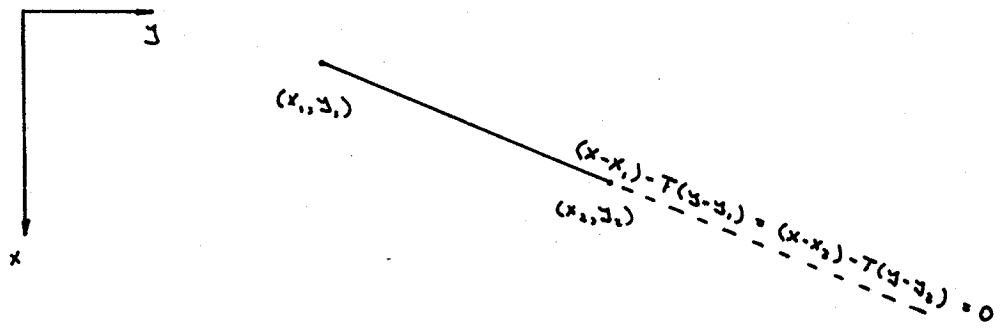

Control points which are near the extension of this edge will have large u and v velocities induced upon them. The singularity can be eliminated by using panels which have a source distribution which varies linearly in the chordwise direction. The resulting continuous source distribution eliminates the singularities. The linearly varying source panel influence equations can be found by integrating the constant source panel influence equations with respect to x.

$$u_{10}=-\frac{k}{2\pi}\left\{y\frac{1}{2}\log\frac{R+x}{R-x}+\frac{(x-Ty)}{\sqrt{T^2+\beta^2}}\frac{1}{2}\log\frac{\sqrt{T^2+\beta^2}R+(Tx+\beta^2y)}{\sqrt{T^2+\beta^2}R-(Tx+\beta^2y)}+z\tan^{-1}\frac{zR}{xy-T(y^2+z^2)}\right\}$$

$$v_{10}=-\frac{k}{2\pi}\left\{(x-Ty)\frac{1}{2}\log\frac{R+x}{R-x}-\frac{T(x-Ty)}{\sqrt{T^2+\beta^2}}\frac{1}{2}\log\frac{\sqrt{T^2+\beta^2}R+(Tx+\beta^2y)}{\sqrt{T^2+\beta^2}R-(Tx+\beta^2y)}-Tz\tan^{-1}\frac{zR}{xy-T(y^2+z^2)}-R\right\}$$

$$w_{10}=-\frac{k}{2\pi}\left\{(x-Ty)\tan^{-1}\frac{zR}{xy-T(y^2+z^2)}+Tz\frac{1}{2}\log\frac{R+x}{R-x}-z\sqrt{T^2+\beta^2}\frac{1}{2}\log\frac{\sqrt{T^2+\beta^2}R+(Tx+\beta^2y)}{\sqrt{T^2+\beta^2}R-(Tx+\beta^2y)}\right\}$$

These velocity components satisfy the same criteria as the velocity components for the constant source panels except that the source strength is proportional to x-Ty. The source panel finite elements are constructed with the following properties.

1. All panel leading and trailing edges are at constant $(\frac{x}{c})$, side edges are at constant y.

2. Each source finite element is composed of a pair of chordwise adjacent panels.

3. The source strength varies linearly with chord measured from the leading edge of a panel pair, i.e. the maximum value of the source strength is proportional to the local chord and attains this maximum on the panel edge joining the panel pair.

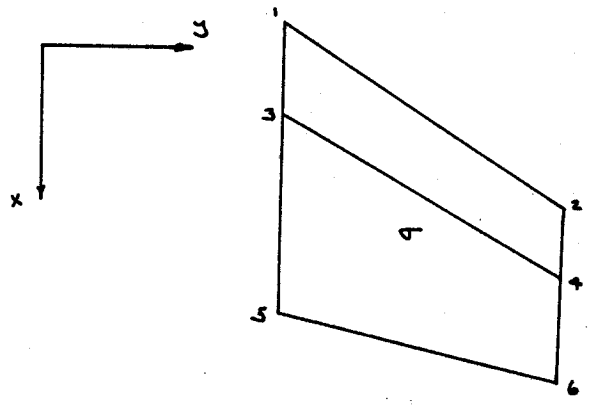

$$\Delta_{31} = \left(\frac{x}{c}\right)_3 - \left(\frac{x}{c}\right)_1 = \left(\frac{x}{c}\right)_4 - \left(\frac{x}{c}\right)_2$$

$$\Delta_{53} = \left(\frac{x}{c}\right)_5 - \left(\frac{x}{c}\right)_3 = \left(\frac{x}{c}\right)_6 - \left(\frac{x}{c}\right)_4$$

The perturbation velocities induced by this panel pair are composed of contributions from six corners.

$$\begin{aligned} u(x,y,z) = \frac{\sigma}{\Delta_{31}} \Big\{ & u_{10}(x-x_1, y-y_1, z, T_1) - u_{10}(x-x_3, y-y_3, z, T_3) \\ & - u_{10}(x-x_2, y-y_2, z, T_2) + u_{10}(x-x_4, y-y_4, z, T_4) \Big\} \\ + \frac{\sigma}{\Delta_{53}} \Big\{ & u_{10}(x-x_5, y-y_5, z, T_5) - u_{10}(x-x_3, y-y_3, z, T_3) \\ & - u_{10}(x-x_6, y-y_6, z, T_6) + u_{10}(x-x_4, y-y_4, z, T_4) \Big\} \end{aligned}$$

If there are N panels in the chordwise direction there will be N-1 singularities or unknown source strengths associated with them. The linear variation in the source distribution means the value of dz/dx must be zero at the leading and trailing edges of each span station. This may be an undesired restriction and therefore the use of linearly varying source panels is optional.

Numerical Solution

Householder's method for solving simultaneous equations is used in the solution of the aerodynamic influence equations. The influence matrix is triangularized by means of orthogonal transformation matrices, which preserve the conditioning of the matrix. This along with a reduction in the number of required computer operations greatly improves the numerical accuracy and stability of the solution over that of the standard Gaussian reduction method.

A complete derivation of the method is given in reference (6). The method has been altered[7] from the original to allow the operation on a single row of the matrix at a time. This reduces the required core allocation necessary to triangularize the matrix.

If [A] is the square influence matrix, the upper triangle is given by

$$[R] = [W][A]$$

where [W] is the combined orthogonal transformation matrix used by Householder to triangularize [A].

In the Householder method [W] is equal to the product of N individual orthogonal transformation matrices, where N equals the number of unknowns. Each transformation results in reducing all elements below the diagonal to zero for one column. The columns are reduced from left to right.

The individual transformation matrices $[W]_m$ are defined by

$$[W]_m = ([I] - 2\{u_m\}\{u_m\}^T)$$

where [I] is a unit diagonal matrix and $\{u_m\}$ is a column matrix defined by the unit vector $\vec{u}_m = (\vec{a}_m - \alpha_m \vec{v}_m)/\mu_m$. The vector $\vec{a}_m$ is defined by the mth column of [A] where the elements on rows less than m are replaced by zeros. The unit vector $\vec{v}_m$ is defined by a column matrix $\{v_m\}$ with all zeros except for the mth row, which is equal to one. The constants α_m and μ_m are defined as

$$\alpha_m = \pm \|\{a_m\}\|$$

$$\mu_m = \sqrt{2\alpha_m(\alpha_m - \vec{v}_m \cdot \vec{a}_m)}$$

It can be shown that $|a_m|$ is reduced to $|\{a_m\}|\ \{v_m\}$ if $\{a_m\}$ is premultiplied by $([I] - 2\{u_m\}\{u_m\}^T)$. Also, that the first m-1 rows of

$$[W_{m-1}][W_{m-2}] \cdots [W_1][A]$$

remain unchanged by the mth transformation. The result after m transformations is then zeros below the diagonal for the first m columns and $|\{a\}_1|$, $|\{a\}_2|$ . ... , $|\{a\}_{m-2}|$, $|\{a\}_{m-1}|$, $|\{a\}_m|$ on the diagonal. The elements above the diagonal have been defined by the m preceding transformations and will remain unchanged for the N-m remaining transformations.

The relation

$$([I] - 2|u_m|\{u_m\}^T)\,|a_m| = |\{a_m\}||v_m| \tag{12}$$

where $\vec{u}_m = (\vec{a}_m - \alpha_m \vec{v}_m)/\mu_m$ or $|u_m| = (|a_m| - \alpha_m|v_m|)/\mu_m$

$$\alpha_m = ||\{a_m\}||$$

and

$$\mu_m = \sqrt{2\alpha_m(\alpha_m - \vec{v}_m \cdot \vec{a}_m)} \quad \text{or} \quad \mu_m = \sqrt{2\alpha_m(\alpha_m - |a_m|^T|v_m|)}$$

remain to be proved. It is helpful in the derivation of equation (12) if the vector identity

$$|\vec{a}_m|\vec{v} + 2(\vec{u}_m \cdot \vec{a}_m)\,\vec{u}_m = \vec{a}_m \tag{13}$$

is observed from the following vector diagram.

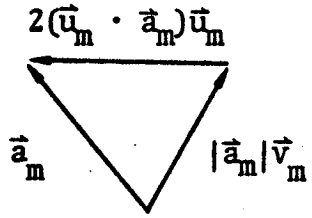

Then from equation (13)

$$|\vec{a}_m|\vec{v}_m + 2\,\vec{u}_m(\vec{u}_m \cdot \vec{a}_m) = \vec{a}_m$$

$$|\vec{a}_m|\vec{v}_m + 2\,\vec{u}_m\vec{u}_m \cdot \vec{a}_m = \vec{a}_m$$

Therefore

$$|\vec{a}_m|\vec{v}_m = (\hat{i}_m\hat{i}_m - 2\,\vec{u}_m\vec{u}_m)\,\vec{a}_m \qquad (14)$$

where $\hat{i}_m\hat{i}_m$ and $\vec{u}_m\vec{u}_m$ are dyadics. The unit vector $\hat{i}_m$ is in the direction of $\vec{a}_m$.

Equation (14) can then be written in matrix notation as follows

$$([I] - 2\,\{u_m\}\{u_m\}^T)\{a_m\} = ||\{a_m\}||\{v_m\}$$

which is equal to equation (12). In matrix or tensor notation it becomes evident that the dimensions of $\{a_m\}$, $\{v_m\}$, and $\{u_m\}$ are not limited to three.

$$\alpha_m = ||\{a_m\}||$$

and

$$\mu_m = 2\,\{u_m\}^T\{a_m\}$$

Then if equation (12) is premultiplied by $\{a_m\}^T$

$$\{a_m\}^T\{a_m\} - 2\{a_m\}^T\{u_m\}\{u_m\}^T\{a_m\} = ||\{a_m\}||\{a_m\}^T\{v_m\} \qquad (15)$$

And substituting α_m and μ_m into equation (15)

$$\alpha^2_m - \frac{1}{2}\mu^2_m = \alpha_m \{a_m\}^T\{v_m\}$$

or

$$\mu_m = \sqrt{2\alpha_m(\alpha_m - \{a_m\}^T\{v_m\})} \tag{16}$$

In vector notation equation (16) is seen to be equal to

$$\mu_m = \sqrt{2\alpha_m(\alpha_m - \vec{v}_m \cdot \vec{a}_m)}$$

Also, if equation (16) is substituted back into equation (12)

$$\{a_m\} - \sqrt{2\alpha_m(\alpha_m - \{a_m\}^T\{v_m\})}\ \{u_m\} = \alpha_m\{v_m\}$$

Therefore

$$\{u_m\} = \frac{\{a_m\} - \alpha_m\{v_m\}}{\sqrt{2\alpha_m(\alpha_m - \{a_m\}^T\{v_m\})}}$$

or in vector notation

$$\vec{u}_m = \frac{\vec{a}_m - \alpha_m \vec{v}_m}{\sqrt{2\alpha_m(\alpha_m - \vec{v}_m \cdot \vec{a}_m)}}$$

Jet Flap

A completely linearized approach was used based on the assumptions of thin airfoil theory. The flow was assumed to be inviscid and irrotational and all entrainment effects were neglected. The jet was represented by an infinitesimally thin sheet having zero mass flow but finite momentum per unit of span. This sheet was assumed to extend from the trailing edge of the surface back to infinity. (In practice one or two chord lengths is sufficient). The effects of transverse momentum and the deflection of the jet sheet were neglected.

Since both the planform and jet can maintain a pressure discontinuity, they are both represented by a system of quadrilateral panels having continuous distributions of vorticity. The strengths of these constant pressure vortex panels are determined by solving a set of linear simultaneous equations which satisfy the downwash boundary conditions at a set of control points on the planform and jet.

The boundary condition on the planform is the previously described flow tangency condition. The pressure difference across the jet causes a change in the direction of the jet momentum. The equation relating these quantities forms the boundary condition on the jet and can be derived by considering a jet segment of unit depth.

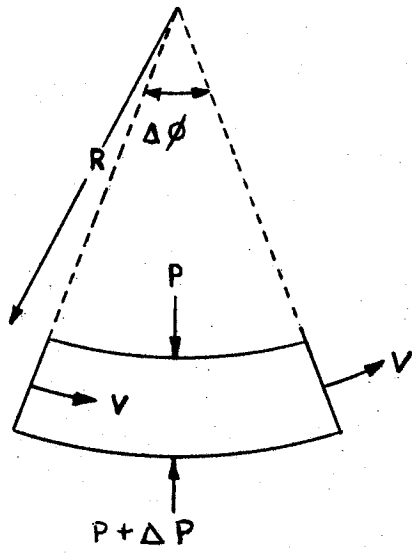

The mass rate of flow through the jet is m and the velocity is V. If we assume a pressure difference of ΔP across the jet, then from the momentum

theorem applied to the differential element, we write

$$mV\,\Delta\phi = \Delta P R\,\Delta\phi$$

or

$$\Delta P = \frac{mV}{R}$$

where R is the radius of curvature of the jet.

The reaction of the jet on the flow external to the jet is

$$F = \Delta P\, R\Delta\phi$$

A vortex of strength per unit length along the jet of γ would produce a reaction of

$$F = \rho U_\infty \gamma R\Delta\phi$$

Hence, equating these two forces, we calculate the action of the jet on the flow external to the jet by replacing the jet with a running vortex strength γ given by

$$\gamma = \frac{mV}{\rho U_\infty R}$$

For a nearly horizontal jet with a large radius of curvature

$$\frac{1}{R} \approx \frac{d^2Z}{dX^2} = \frac{dw}{dX}$$

where w is local downwash velocity (nondimensionalized with respect to U_∞).

Then

$$\frac{1}{2} C_{p_{NET}} = \frac{\gamma}{U_\infty} = \frac{1}{2}\rho U_\infty^2 C\left(\frac{mV}{qC}\right)\frac{1}{\rho U_\infty^2}\frac{dw}{dX}$$

or

$$C_\mu(Y)\,C(Y)\,\frac{\partial w}{\partial X}(X,Y) - C_{P_{NET}}(X,Y) = 0$$

which is the boundary condition written for a three dimensional jet flap.

To apply the jet flap boundary condition to control point i, the above equation is integrated between adajacent control points in the streamwise direction.

$$C_\mu(Y)\,C(Y)\int_{X_{c_{i-1}}}^{X_{c_i}} \frac{\partial w}{\partial X}(X,Y)\,dX - \int_{X_{c_{i-1}}}^{X_{c_i}} C_{P_{NET}}(X,Y)\,dX = 0 \qquad (17)$$

The control point is located at 87.5 percent of each panel chord. To simplify the second integral in equation (17) the assumption is made that the control point is exactly at the panel trailing edge. The effects of such an assumption have been shown to be negligible. Equation (17) evaluated from the leading to the trailing edge of panel i yields the following relation:

$$C_\mu C\left[w_i - w_{i-1}\right] - C_{P_{NET_i}}\,\Delta X_i = 0 \qquad (18)$$

The downwash at each control point is written in terms of the N net pressures on the quadrilateral panels:

$$w_i = \sum_{j=1}^{N} A_{ij}\,C_{P_{NET_j}}$$

$$w_{i-1} = \sum_{j=1}^{N} A_{i-1\,j}\,C_{P_{NET_j}}$$

Equation (18) is then written

$$\sum_{j=1}^{N} \left\{C_\mu C\left[A_{ij} - A_{i-1\,j}\right] - \delta_{ij}\Delta X_i\right\} C_{P_{NET_j}} = 0$$

where δ_{ij} is the Kroneker delta.

For a flap panel adjacent to the jet exit, equation (18) must include any jet deflection angle relative to the surface trailing edge.

$$C_\mu C \left[w_i - (w_{i-1} + \delta_j)\right] - C_{P_{NET_i}} \Delta X_i = 0$$

or

$$C_\mu C \left[w_i - w_{i-1}\right] - C_{P_{NET_i}} \Delta X_i \Big\} C_{P_{NET_j}} = C_\mu C \delta_j$$

where δ_j is the jet deflection angle.

Then

$$\sum_{j=1}^{N} C_\mu C \left\{\left[A_{ij} - A_{i-1\,j}\right] - \delta_{ij} \Delta X_i\right\} C_{P_{NET_j}} = C_\mu C \delta_j$$

The complete set of linear simultaneous equations for both the surface and the jet flap is then written

$$\sum_{j=1}^{N} A_{ij} \; C_{P_{NET_j}} = C_i \qquad i = 1, N \qquad (19)$$

where

$$A_{ij} = \begin{cases} A_{ij} & \text{for i on the surface} \\ C_\mu C \left[A_{ij} - A_{i-1\,j}\right] - \delta_{ij} \Delta X_i & \text{for i on the jet} \end{cases}$$

and $C_i = \begin{cases} -\alpha_i & \text{for i on the surface} \\ C_\mu C r_i & \text{for i on the jet adjacent to the exit} \\ 0 & \text{for i elsewhere on the jet} \end{cases}$

Both symmetric and antisymmetric jet deflections are considered. Thus after calculating the influence matrices and boundary conditions in the usual manner, the appropriate rows are modified and combined to produce a linear symmetric or antisymmetric system as described by equation (19). Because of the rotational quality of the flow fields, the p, q and r rotary derivative calculations are generally not valid for jet flap configurations.

AERODYNAMIC CHARACTERISTICS

Longitudinal and lateral-directional forces and moments due to thickness, twist and camber, pitch, sideslip, and the dimensionless rotary velocities $\hat{p}$, $\hat{q}$, $\hat{r}$ are obtained from surface pressure integrations of the various configuration components.

Bodies

The pressure coefficient, to an approximation consistant with slender body theory, is

$$C_p = \frac{P-P_\infty}{q} = -2\left\{\phi_x + g'(x) + \left[\alpha + \hat{q}\,\frac{(x-CG)}{c/2} + \hat{P}\,\frac{Y}{b/2}\right]\phi_Z - \left[\beta - \hat{r}\,\frac{(x-XCG)}{b/2} + \hat{P}\,\frac{(z-z_{C.G.})}{b/2}\right]\phi_Y\right\} - \phi_Y^2 - \phi_Z^2 \tag{20}$$

The forces and moments are obtained from the surface integrations

$$\frac{F_x}{qL^2} = \int_c^1 dx \oint C_p \frac{\partial y}{\partial x}\, ds$$

$$\frac{F_Y}{qL^2} = -\int_0^1 dx \oint C_p\, dz$$

$$\frac{F_z}{qL^2} = \int_0^1 dx \oint C_p\, dY$$

$$\frac{M_x}{qL^3} = -\int_0^1 dx \oint (z-z_{CG})\, C_p\, dz - \int_0^1 dx \oint Y\, C_p\, dY$$

$$\frac{M_Y}{qL^3} = -\int_0^1 (x-x_{CG})\, dx \oint C_p\, dY$$

$$\frac{M_z}{qL^3} = \int_0^1 (x-x_{CG})\, dx \oint C_p\, dz$$

In terms of these expressions, the commonly used aerodynamic coefficients are

$$C_x = \frac{F_x}{qL^2} \cdot \frac{L^2}{S_{REF}}$$

$$C_Y = \frac{F_Y}{qL^2} \cdot \frac{L^2}{S_{REF}}$$

$$C_z = \frac{F_z}{qL^2} \cdot \frac{L^2}{S_{REF}}$$

$$C_l = \frac{M_x}{qL^3} \frac{L^3}{b\ S_{REF}}$$

$$C_m = \frac{M_Y}{qL^3} \frac{L^3}{\bar{c}\ S_{REF}}$$

$$C_n = \frac{M_z}{qL^3} \frac{L^3}{b\ S_{REF}}$$

where L is the body length and $\bar{c}$, b and S_{ref} are configuration reference chord, span and area respectively.

Crosscoupling between the pitch, sideslip, and rotary motions through the product and quadratic terms in equation (20) is neglected.

Planar Components

Surface pressure distributions are calculated for planar components using the first-order linearized form of the pressure coefficient.

$$C_p = -\frac{2u}{U} = -2\left[\frac{u}{U}_{IND} \pm \frac{C_{P_{NET}}}{4}\right]$$

The +/- signs refer to the upper and lower surfaces respectively. The term $\frac{u}{U}_{IND}$ consists of the velocities induced by the isolated bodies and other vortex and source panels. These velocities are obtained by multiplying the $\frac{u}{U}$ influence matrices by the appropriate panel strengths. The $C_{P_{NET}}/4$ term accounts for the $\frac{u}{U}$ perturbation velocity induced by the local distribution of vorticity and changes sign from upper to lower surface. The total $\frac{u}{U}$ and $C_{P_{NET}}$ values are the result of taking linear combinations of all the basic and unit solutions.

The net pressures for each of the basic and unit solutions are integrated numerically to give the section forces and moments, component forces and moments and configuration forces and moments.

Since the vortex panels have a constant pressure distribution, a block integration scheme is employed. With the exception of drag, these basic and unit force and moment coefficients are combined in a linear manner to produce the aerodynamic characteristics for any desired flight condition. Since drag varies in a parabolic manner, it must be considered on a point by point basis as defined in a later section.

The longitudinal normal force distribution on the bodies in calculated for each solution. The load distribution on the interference shell portion of the body is given by integrating over all vortex panels at a given longitudinal station.

normal force

$$C_n \frac{w}{\ell} = \frac{C_1}{\Delta X\, L} \sum_{i=1}^{N} C_{P_{NET_i}} A_i \cos\Theta_i$$

where N is the number of panels around the shell, L is the length of the body, ΔX is the length of the interference shell segment, A_i is the panel area and $C_1 = 2$ for a centerline body or $C_1 = 1$ for an off centerline body. This carryover load distribution is added to the previously calculated isolated body longitudinal load distribution.

The section characteristics of planar components are determined by a chordwise summation of panel data at each span station and are given by the following equations:

local lift coefficient

$$C_n = \frac{1}{C \Delta s} \sum_{i=1}^{N} C_{P_{NET_i}} A_i$$

normal force

$$C_n \frac{C}{C_{AVG}} = \frac{1}{\Delta s \, C_{AVG}} \sum_{i=1}^{N} C_{P_{NET_i}} A_i$$

lift force

$$C_\ell \frac{C}{C_{AVG}} = \frac{1}{\Delta s C_{AVG}} \sum_{i=1}^{N} C_{P_{NET_i}} A_i \cos \theta_i$$

center of pressure

$$X_{C.P.} = \frac{\frac{1}{C \Delta s C_{AVG}} \sum_{i=1}^{N} C_{P_{NET_i}} A_i (x_i - X_{LE})}{C_n \frac{C}{C_{AVG}}}$$

where N is the number of chordwise panels, and Δs is the width of the span station and is given by

$$\Delta s = \sqrt{\Delta Y^2 + \Delta Z^2}$$

The section characteristics due to the reaction of a jet flap are calculated by taking the appropriate component of the reaction force.

reaction normal force

$$C_n \frac{C}{C_{AVG}} = C_\mu \frac{C}{C_{AVG}} \sin \delta_{jT} \approx C_\mu \frac{C}{C_{AVG}} \delta_{jT}$$

where δ_{jT} is the total deflection angle of the jet.

reaction lift force

$$C_\ell \frac{C}{C_{AVG}} = C_n \frac{C}{C_{AVG}} \cos \Theta$$

Component forces and moments (excluding jet reaction loads) are given by the following equations:

lift

$$C_L = \frac{F_1}{S_{REF}} \sum_{i=1}^{N} C_{P_{NET_i}} A_i \cos \theta_i$$

side force

$$C_Y = -\frac{F_2}{S_{REF}} \sum_{i=1}^{N} C_{P_{NET_i}} A_i \sin \theta_i$$

rolling moment

$$C_\ell = \frac{-F_2}{bS_{REF}} \sum_{i=1}^{N} C_{P_{NET_i}} A_i \left[\cos\theta_i \left(Y_i - Y_{CG}\right) + \sin\theta_i \left(z_i - Z_{CG}\right) \right]$$

pitching moment

$$C_m = \frac{-F_1}{\bar{c}\, S_{REF}} \sum_{i=1}^{N} C_{P_{NET_i}} A_i \cos\theta_i \left(x_i - X_{CG}\right)$$

yawing moment

$$C_n = \frac{F_2}{b\, S_{REF}} \sum_{i=1}^{N} C_{P_{NET_i}} A_i \sin\theta_i \left(x_i - X_{CG}\right)$$

where N is the total number of vortex panels on the component, and F_1 and F_2 are defined as follows:

symmetric loading

$F_1 = 1$ asymmetric geometry

$= 2$ symmetric geometry

$F_2 = 1$ asymmetric geometry

$= 0$ symmetric geometry

antisymmetric loading

$F_1 = 1$ asymmetric geometry

$= 0$ symmetric geometry

$F_2 = 1$ asymmetric geometry

$= 2$ symmetric geometry

The X coordinate of the center of pressure is given by

$$X_{C.P.} = -\frac{C_m \bar{c}}{C_L} + X_{CG}$$

For interference shell components, the total forces and moments of the corresponding isolated body are added to those of the shell.

Jet reaction forces and moments are obtained from a spanwise summation of the jet flap section characteristics:

lift

$$C_{L_{JET}} = \frac{F_1}{S_{REF}} \sum_{i=1}^{N} (C_\mu C)_i \, \delta_{jT_i} \, \Delta s_i \cos \theta_i$$

side force

$$C_{Y_{JET}} = \frac{-F_2}{S_{REF}} \sum_{i=1}^{N} (C_\mu C)_i \, \delta_{jT_i} \, \Delta s_i \sin \theta_i$$

rolling moment

$$C_{\ell_{JET}} = \frac{-F_2}{b \, S_{REF}} \sum_{i=1}^{N} (C_\mu C)_i \, \delta_{jT_i} \, \Delta s_i \times \left[\cos \theta_i (Y_i - Y_{CG}) + \sin \theta_i (Z_i - Z_{CG}) \right]$$

pitching moment

$$C_{m_{JET}} = \frac{-F_1}{\bar{c} \, S_{REF}} \sum_{i=1}^{N} (C_\mu C)_i \, \delta_{jT_i} \, \Delta s_i \cos \theta_i (X_i - X_{CG})$$

yawing moment

$$C_{n_{JET}} = \frac{F_2}{b\,S_{REF}} \sum_{i=1}^{N} (C_\mu C)_i\, \delta_{jT_i}\, \Delta s_i\, \sin\theta_i\, (x_i - x_{CG})$$

where N is the number of spanwise jet flap stations and F_1 and F_2 are defined as before.

The forces and moments for the complete configuration are obtained by summing those of the individual components.

DRAG ANALYSIS

Preliminary estimation of configuration aerodynamic efficiency requires the calculation of aerodynamic drag. The program separates the computation into two parts which are assumed to be independent of each other: viscous skin friction drag and pressure drag. The latter calculation results in a set of drag polars representing the attainment of zero or one hundred percent of the leading edge suction available. The complete estimation of the pressure drag requires an assessment of the percent of leading edge suction which can be attained. Although the loss of "suction" is due to viscous effects, it is assumed the suction level will be estimated semi-empirically and therefore is not part of the viscous calculation. Trim drag polars may be calculated to assess the tradeoff between longitudinal stability and performance.

The calculation procedure assumes the viscous skin friction drag and supersonic pressure drag due to thickness are independent of lift. The use of a linearized analysis results in a quadratic drag polar for the drag due to lift. Therefore the trimmed or untrimmed drag polar for zero suction or one hundred percent suction is of the form

$$C_D = C_{D_{VISCOUS}} + C_{D_{THICKNESS}} + C_{D_{MIN}} + K(C_L - C_{L_{MIN}})^2$$

where K depends on the type of polar. The specific techniques used to accomplish the drag analysis are discussed below.

Skin Friction

Several well established semiempirical techniques for the evaluation of adiabatic laminar and turbulent flat plate skin friction at incompressible and compressible speeds are used to estimate the viscous drag of advanced aircraft using a component buildup approach. A specified transition point calculation option is provided for in conjunction with a matching of the momentum thickness to link the two boundary layer states. For the turbulent condition, the increase in drag due to distributed surface roughness is treated using unformly distributed sand grain results. Component thickness effects are approximated using experimental data correlations for two-dimensional airfoil sections and bodies of revolution.

Considerations such as separation, component interference, and discrete protuberances (e.g. antennas, drains, aft facing steps, etc.) must be accounted for separately if present.

In the following, a discussion is presented for a single component evaluation in order to simplify writing of the equations and eliminate multiple subscripting. The total result is obtained by a surface area weighted summation of the various component analyses as described on page 63.

Laminar/Transition

A specified transition option is provided in the program. The principal function of the calculation is to provide the conditions required to initialize the turbulent solution. In particular, the transition point length and momentum thickness Reynolds numbers are required.

$$R_{x_{TRAN}} = R \frac{x_{TRAN}}{L} L$$

$$R_{\theta_{TRAN}} = 0.664 \sqrt{R_{x_{TRAN}} C^*}$$

where

$$C^* = \frac{\mu^*}{\mu_\infty} \frac{T_\infty}{T^*}$$

$$\frac{T^*}{T_\infty} = 1 + 0.72 \left[\frac{T_r}{T_\infty} - 1 \right]$$

$$\frac{T_r}{T_\infty} = 1 + \sqrt{P_r} \frac{\gamma - 1}{2} M_\infty^2 = 1 + 0.851 \frac{\gamma - 1}{2} M_\infty^2$$

$$\mu = 2.270 \times 10^{-8} \frac{T^{3/2}}{T + 198.6} \quad \text{lb sec/ft}^2$$

This solution is based on the laminar Blasius result (8, chapter VII) in conjunction with Eckert's compressibility transformation[9]. This option permits an assessment of the reduction in skin friction drag if laminar flow can be maintained for the specified extent. It does not establish the liklihood that such a condition will be realized in practice or to what extent.

Turbulent

Smooth and distributed rough surface options have been provided in the analysis. In either case, the solution is initialized by matching the momentum thickness at the transition point produced by the laminar/transition solution. That is, an effective origin (commonly referred to as a virtual origin) is established for the turbulent analysis.

For the hydraulically smooth case

$$C_F R_{\Delta X} = 2 R_{\theta_{TRAN}}$$

$$R_{\Delta X} = C_F R_{\Delta X} / C_F \qquad C_F \text{ from equation (21) for known } C_F R_{\Delta X}$$

$$\Delta X = R_{\Delta X} / R$$

$$\ell = L - X_{TRAN} + \Delta X$$

$$R_\ell = R \ell$$

$$\frac{0.242 \left[\sin^{-1}\alpha + \sin^{-1}\beta \right]}{\left[\frac{\gamma-1}{2} M_\infty^2 C_F' \right]^{\frac{1}{2}}} = \log_{10} \left[C_F' R_\ell \right] - \omega \log_{10} \frac{T_w}{T_\infty} \qquad (21)$$

$$C_F = \frac{2\theta_{x\to\infty}}{L} = \frac{2\theta_{T.E.}}{\ell} \frac{\ell}{L} = C_F' \frac{\ell}{L}$$

where

$$X_{TRAN} = R_{X_{TRAN}} / R$$

$$\alpha = (2A^2 - B) / \sqrt{B^2 + 4A^2}$$

$$\beta = B / \sqrt{B^2 + 4A^2}$$

$$A^2 = \frac{\gamma - 1}{2} M_\infty^2 \frac{T_\infty}{T_r}$$

$$B = \left(1 + \tfrac{1}{2}[\gamma - 1] M_\infty^2\right) \frac{T_\infty}{T_r} - 1$$

$$r = 0.88$$

$$\omega = 0.76$$

The compressible turbulent flat plate method used here is that proposed by Van Driest[10] based on the Von Karman mixing length hypothesis in conjunction with the Squire-Young formulation for profile drag (8 , chapter XXIV) as applied to a flat plate.

For the distributed rough case

$$\Delta X_1 = X_{TRAN}$$

$$C_{F_r} = \left[1.89 + 1.62 \log_{10} \frac{\Delta X}{K_s} \right]^{-2.5} \left(1 + r \frac{\gamma - 1}{2} M_\infty^2 \right)^{-1}$$

$$R_{\Delta X_{i+1}} = 2 R_{\theta_{TRAN}} / C_{F_r}$$

$$\Delta X_{i+1} = R_{\Delta X_{i+1}} / R$$

$$\ell = L - X_{TRAN} + \Delta X$$

$$C_F' = \left(1.89 + 1.62 \log_{10} \frac{\ell}{K_s} \right)^{-2.5} \left(1 + r \frac{\gamma - 1}{2} M_\infty^2 \right)^{-1}$$

$$C_F = C_F' \frac{\ell}{L}$$

$$C_F = MAX \left[C_{F_{SMOOTH}}, C_{F_{ROUGH}} \right]$$

The turbulent flat plate method used here is that of Schlicting (8, chapter XXI) which is based on a transposition of Nikuradse's densely packed sand grain roughened pipe data. The effect of compressibility is due to the reduction in density at the wall as proposed by Goddard.[11] The selection of the equivalent sand grain roughness for a given manufacturing surface finish is made with the aid of Table II which was taken from Clutter.[12]

TABLE II

Type of Surface	Equivalent Sand Roughness K_s (inches)
Aerodynamically smooth	0
Polished metal or wood	$0.02 - 0.08 \times 10^{-3}$
Natural sheet metal	0.16×10^{-3}
Smooth matte paint, carefully applied	0.25×10^{-3}
Standard camouflage paint, average application	0.40×10^{-3}
Camouflage paint, mass-production spray	1.20×10^{-3}
Dip-galvanized metal surface	6×10^{-3}
Natural surface of cast iron	10×10^{-3}

Thickness Corrections

The foregoing evaluations produce as estimate of the shearing forces on a flat plate (at zero angle of attack) for a variety of conditions. As an actual aircraft has a non vanishing thickness, an estimate of pressure gradient effects on skin friction and boundary layer displacement pressure drag losses is required. A common procedure for accomplishing this and the one which will be used here is based on non-lifting experimental correlations for symmetric two-dimensional airfoils and axisymmetric bodies. The following relations derived by Horner (13, chapter VI) are used respectively.

$$K = \frac{C_d}{2C_f} = 1 + K_1 \frac{t}{c} + 60\left(\frac{t}{c}\right)^4$$

$$= \frac{C_D}{C_{DF}} = 1 + 1.5\left(\frac{d}{L}\right)^{\frac{3}{2}} + 7\left(\frac{d}{L}\right)^3$$

Horner recommends $K_1 = 2$ for airfoils with maximum thickness at 30% chord and $K_1 = 1.2$ for NACA 64 and 65 series airfoils. In this regard, the best information available to an analyst for his particular contour should be used. This is especially true for modern high performance shapes such as the supercritical airfoil, etc.

Total Viscous Drag

The aircraft total viscous drag coefficient is estimated by a sum of the preceding analysis over all components (i.e. wing, fuselage, vertical tail, etc.). That is

$$C_{D_{VISCOUS}} = \sum_{j=1}^{N} C_{F_j} \left(\frac{S_j}{S_{REF}}\right) K_j$$

The component length used in the calculation of the skin friction coefficient is the mean chord for planar component segments and the physical length for bodies and nacelles.

Zero Suction Drag

The zero suction drag due to lift is calculated by numerically integrating the net pressure distribution times the projected area in the streamwise direction over each of the planer surfaces. The following block integration scheme is used to sum over all quadrilateral panels.

$$C_D = F_1 \frac{1}{S_{REF}} \sum_{i=1}^{N} C_{P_i} A_i \alpha_i$$

where

$$C_{P_i} = C_{P_{i_{\alpha=0}}} + \alpha \frac{\partial C_{P_i}}{\partial \alpha} + \delta \frac{\partial C_{P_i}}{\partial \delta}$$

and

$$\alpha_i = \alpha_{o_i} + \alpha + \sigma_i \delta \qquad @ \ .875\, c$$

α_{o_i} is due to twist and camber, δ is the control surface deflection and $\sigma_i = 1$ for control surface panels and $\sigma_i = 0$ for non control surface panels. $F_1 = 2$ for symmetric geometries and $F_1 = 1$ for asymmetric geometries. For configurations having jet flaps, an additional drag term

must be included to account for the loss in thrust due to the downward deflection of the jet. This drag increment can be seen from the following thrust diagram.

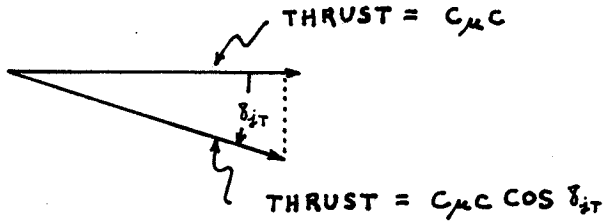

The section thrust loss can be expressed by the equation

$$\frac{1}{\Delta A} S_{REF} \Delta C_D = C_\mu C (1 - \cos \delta_{jT}) \approx \frac{1}{2} C_\mu C \delta_{jT}^2$$

where δ_{jT} is the total deflection angle at the section of interest. The total increment can be found by a spanwise summation of the section thrust loss:

$$\Delta C_D = \frac{F_1}{S_{REF}} \frac{1}{2} \sum_{i=1}^{N} (C_\mu C)_i \Delta A_i \delta_{jT_i}^2$$

Potential Form Drag

One hundred percent suction drag due to lift and supersonic wave drag due to thickness can be evaluated by integration of the momentum flux through a large circular cylinder centered on the x axis and whose radius approaches infinity.

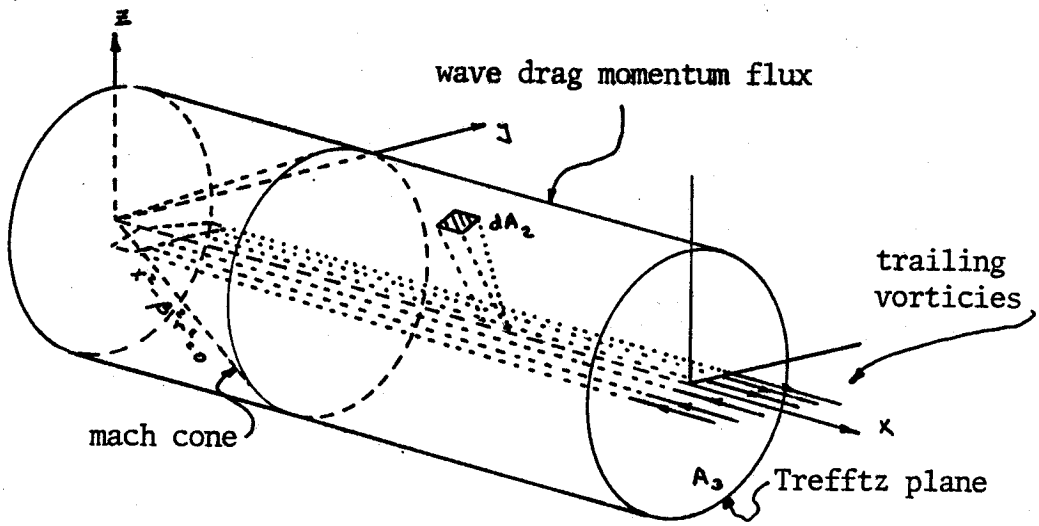

The resulting expression for the total pressure drag is as follows:

$$C_D S_{REF} = -2 \iint_{A_2} \bar{\Phi}_x \bar{\Phi}_v \, dA_2 + \iint_{A_3} (\bar{\Phi}_y^2 + \bar{\Phi}_z^2) \, dA_3$$

The first term represents the wave drag due to momentum losses thru the side of the cylinder caused by standing pressure waves. The second term represents the vortex drag which arises from the kinetic energy left behind in the Trefftz plane by the system of trailing vorticies. Included in the vortex drag is the loss in the axial component of thrust due to a deflected jet flap. The calculation of these terms is discussed below.

Vortex Drag

The vortex drag may be computed when the distribution of trailing vorticity in the Trefftz plane is known. The assumptions of linearized thin wing theory result in a vortex sheet which extends directly downstream of all lifting surfaces. By changing a surface integral for kinetic energy to a line integral over the vortex sheet in the Trefftz plane the following integral for drag results

$$C_D = \frac{1}{b} \int_{-b/2}^{b/2} \left[\bar{C}_N(\Delta) + \bar{C}_m(\Delta) \omega_m(\Delta) \right] \omega_m(\Delta) \, d\Delta$$

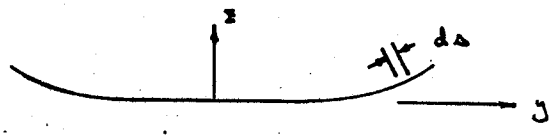

where in addition

$$C_L = \frac{1}{b} \int_{-b/2}^{b/2} \left[\bar{C}_N(\Delta) + \bar{C}_m(\Delta) \omega_m(\Delta) \right] \cos\theta(\Delta) \, d\Delta$$

$$C_T = \frac{1}{b} \int_{-b/2}^{b/2} \bar{C}_m(\Delta) \, d\Delta$$

and where $\bar{C}_N(\Delta)$ is the sectional $c_N c / c_{AVG}$
$\bar{C}_m(\Delta)$ is the sectional $c_m c / c_{AVG}$
$\omega_m(\Delta)$ is the local normal velocity on the vortex sheet in the Trefftz plane
$\theta(\Delta)$ is the local inclination of the sheet with respect to the y axis

The program computes the normal velocity on the vortex sheet, ω_{∞_i}, by assuming the vortex sheet is composed of finite trailing horseshoe vorticies whose strength is proportional to the local section $C_N(s)$. The normal velocity is computed at a control point located midway between the trailing vortex segments.

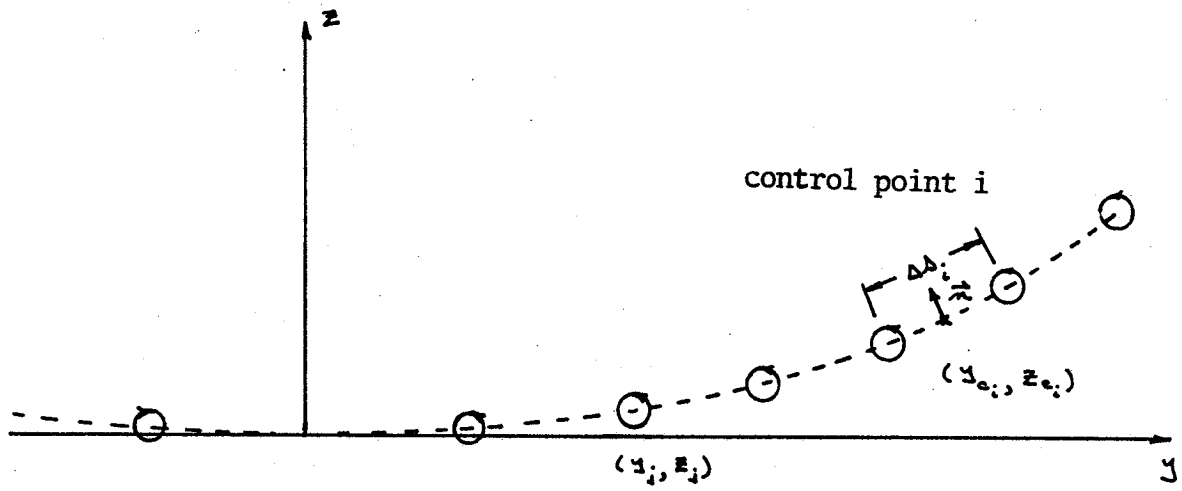

Each vortex j induces a contribution to the normal velocity at section i.

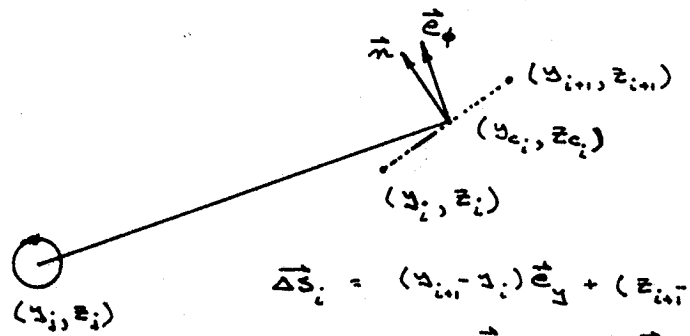

$$\vec{V} = \frac{C_{Ave}\Gamma_j}{2\pi r}\vec{e}_\phi$$

$$\Gamma_j = \frac{1}{2}\left[\bar{C}_{N_j} - \bar{C}_{N_{j+1}}\right]$$

$$\vec{r} = \left[(y_{c_i} - y_j)\vec{e}_y + (z_{c_i} - z_j)\vec{e}_z\right]$$

$$\vec{e}_\phi = \left[-(z_{c_i} - z_j)\vec{e}_y + (y_{c_i} - y_j)\vec{e}_z\right]\frac{1}{r}$$

$$\vec{\Delta s}_i = (y_{i+1} - y_i)\vec{e}_y + (z_{i+1} - z_i)\vec{e}_z$$

$$= \Delta y_i \vec{e}_y + \Delta z_i \vec{e}_z$$

$$\vec{n} = \frac{1}{\Delta s_i}\left[-\Delta z_i \vec{e}_y + \Delta y_i \vec{e}_z\right]$$

$$\omega_{\infty_i} = \vec{V}\cdot\vec{n} = \frac{C_{Ave}}{2\pi r^2 \Delta s_i}\left\{(z_{c_i} - z_j)\Delta z_i + (y_{c_i} - y_j)\Delta y_i\right\}\Gamma_j = A_{ij}\Gamma_j$$

Therefore $$C_D = \sum_i \omega_{\infty_i}\bar{C}_{N_i}\Delta s_i \qquad \omega_{\infty_i} = \sum_j A_{ij}\Gamma_j$$

Wave Drag

The integral for wave drag

$$C_{D_W} S_{REF} = -2 \iint_{A_2} \phi_x \phi_r \, r \, dx \, d\theta$$

may be simplified by allowing the cylindrical surface of integration to recede infinitely far from the disturbance. Under these conditions it is possible to reduce spatial singularity simulations to a series of one-dimensional distributions. The basis for this reduction is the finding by Hayes (14) that the potential and the gradients of interest induced by a singularity along an arbitrary trace on a distant control surface, say PP' of figure 6 (or alternately described by the cylindrical angle θ), is invariant to a finite translation along the surface of a hyperboloid emanating from the trace and passing through the singularity. As the apex of the hyperboloid is a great distance away, the aforementioned movement is along a surface which is essentially plane; it will be henceforth referred to as an "oblique plane". Since a singularity is a solution of a linear differential equation, all singular solutions which lie on the surface of the same hyperboloid (oblique plane) may thus be grouped to form a single equivalent point singularity whose strength is equal to the algebraic sum of the individual strengths and which induces the same potential (momentum) along the trace as the group of individual singularities.

This finding provides the basic technique for reducing a general spatial distribution of singularities to a series of equivalent lineal distributions. This is accomplished by surveying the three-dimensional distribution longitudinally at a series of fixed cylindrical angles, θ . At each angle, the survey produces an equivalent lineal distribution by systematically cutting the spatial distribution at a series of longitudinal stations along its length. At each cut, the group of intercepted singularities is collapsed along the "oblique plane" to form one of the equivalent point singularities comprising the lineal distribution .

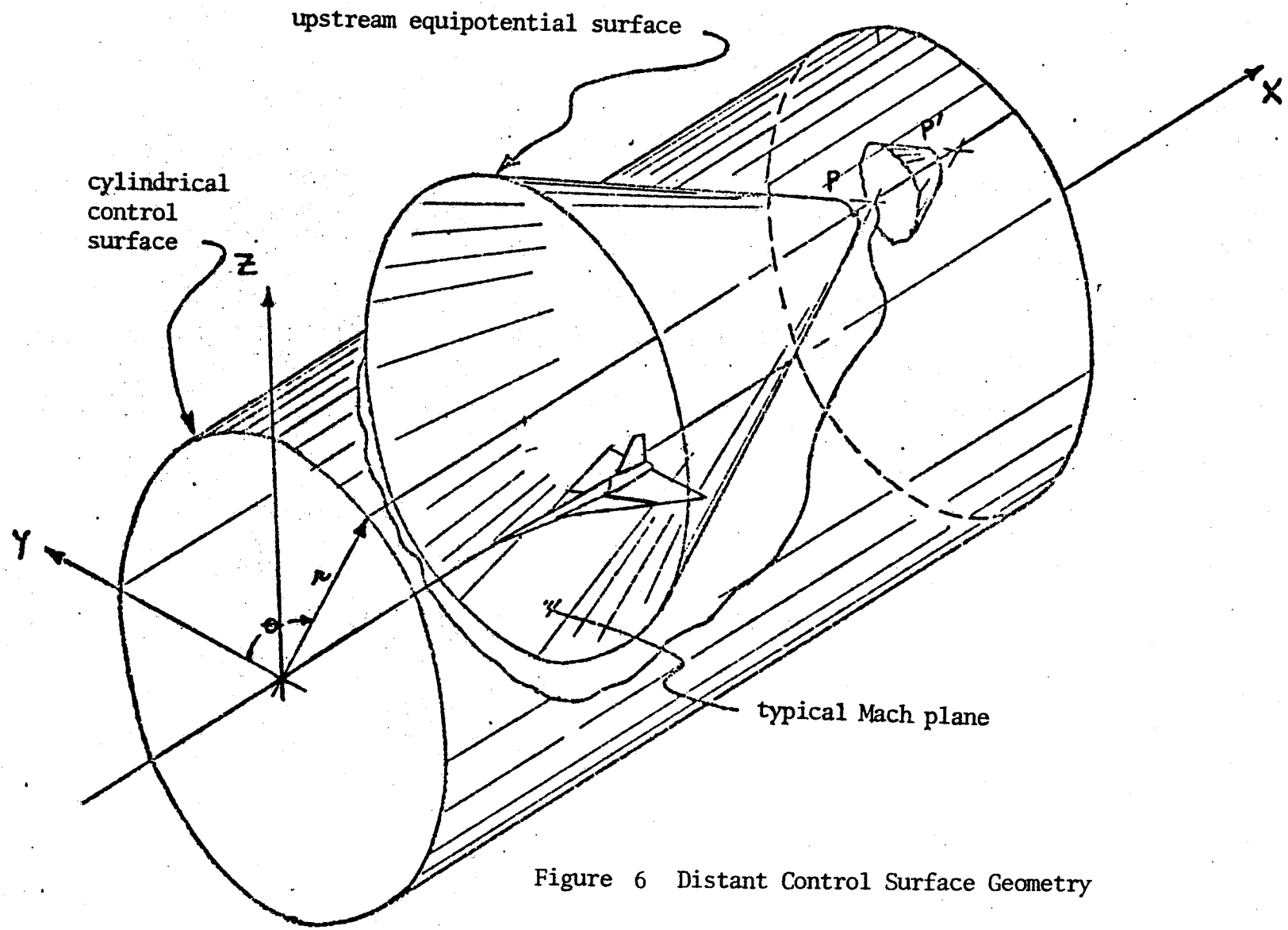

Figure 6 Distant Control Surface Geometry

The far field expression for the wave drag of a general system of lift, and side force elements is

$$C_{D_W} S_{REF} = \frac{1}{U^2} \frac{1}{4\pi^2} \int_0^{2\pi} \int_{-\infty}^{\infty} \int_{-\infty}^{\infty} h_e'(\epsilon_1,\theta)\, h_e'(\epsilon_2,\theta) \ln|\epsilon_1-\epsilon_2|\, d\epsilon_1 d\epsilon_2 d\theta$$

where

$h_e(\epsilon,\theta) = f(\epsilon,\theta) - g_z(\epsilon,\theta)\sin\theta - g_y(\epsilon,\theta)\cos\theta$

is the equivalent lineal singularity strength at the cylindrical angle θ

$f(\epsilon,\theta)$ = equivalent source strength per unit length

$\frac{1}{\beta} U \; g_z(\epsilon,\theta)$ = equivalent lifting element strength per unit length

$\frac{1}{\beta} U \; g_y(\epsilon,\theta)$ = equivalent side force strength per unit length

These strengths are deduced from the three dimensional singularity distributions by application of the superposition principle along equipotential surfaces. For a distant observer such surfaces are planar in the vicinity of the singularity configuration. The individual singularity strengths are related to the object under consideration by the requirement of flow tangency at the solid boundary. Lomax (15) derived the following approximate expressions between the equivalent singularity strengths and a slender lifting object.

$$f(\epsilon,\theta) = U \frac{\partial}{\partial \epsilon} A(\epsilon,\theta)$$

$$g_z(\epsilon,\theta) = \frac{1}{2}\beta U \int_c C_p\, dy$$

$$g_y(\epsilon,\theta) = \frac{1}{2}\beta U \int_c C_p\, dz$$

where (see figure 7)

$A(\epsilon,\theta)$ is the Y-Z projection of the obliquely cut crossectional area

c is the contour around the surface in the oblique cut

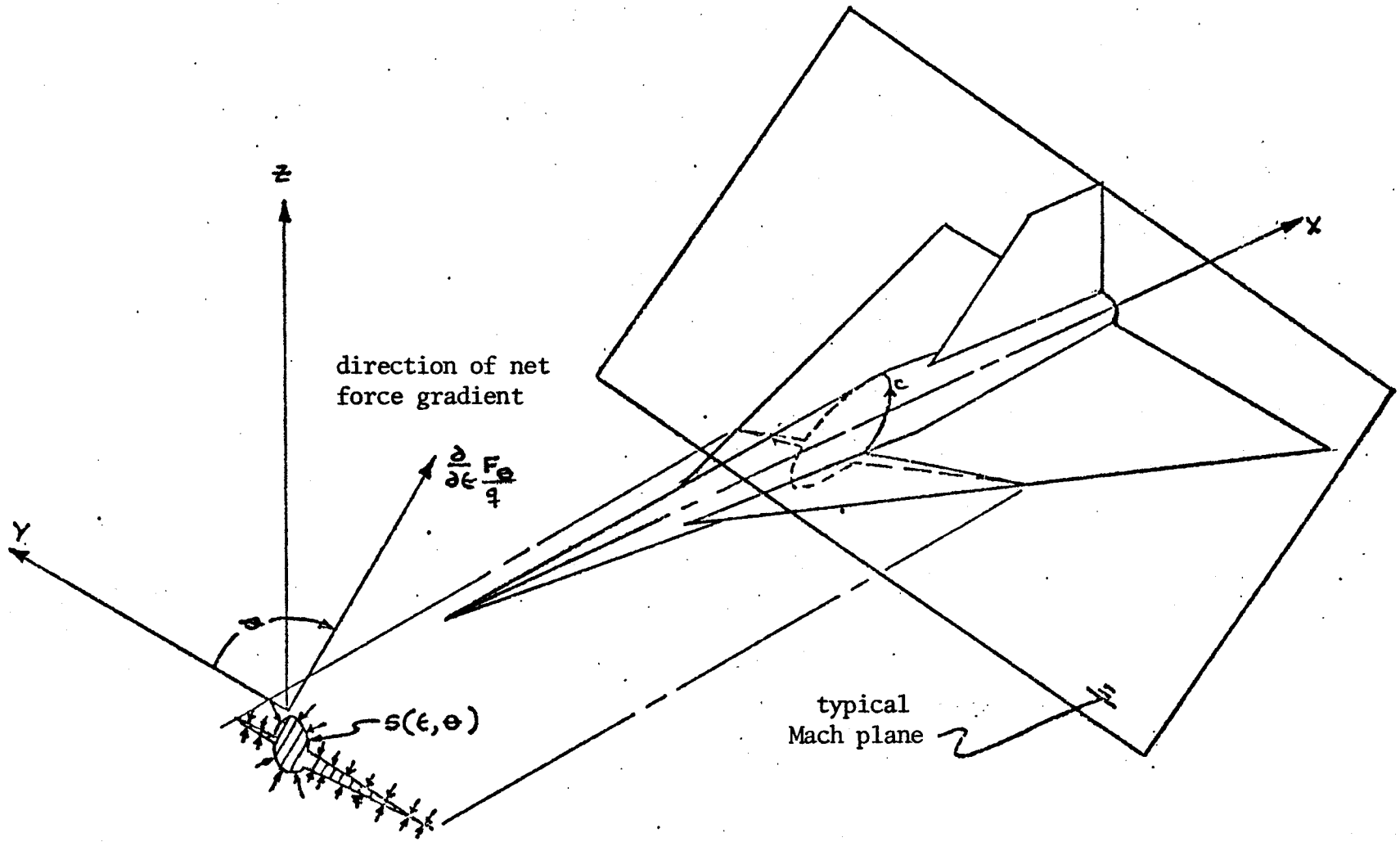

Figure 7 Areas and Forces Pertinent to the Evaluation of Wave Drag from the Far Field Point of View

Utilizing the singularity strength expressions derived by Lomax, the following expression for wave resistance based on the far field theory of Hayes is obtained

$$C_{D_W} S_{REF} = -\frac{1}{4\pi^2} \int_0^{2\pi} \int_0^{L(\theta)} \int_0^{L(\theta)} \left\{ \frac{\partial^2}{\partial \epsilon_1^2} A(\epsilon_1,\theta) - \frac{1}{2}\beta \frac{\partial}{\partial \epsilon_1} \left[\sin\theta \int_c C_p(\epsilon_1,\theta)\,dy + \cos\theta \int_c C_p(\epsilon_1,\theta)\,dz \right] \right\}$$

$$\left\{ \frac{\partial^2}{\partial \epsilon_2^2} A(\epsilon_2,\theta) - \frac{1}{2}\beta \frac{\partial}{\partial \epsilon_2} \left[\sin\theta \int_c C_p(\epsilon_2,\theta)\,dy + \cos\theta \int_c C_p(\epsilon_2,\theta)\,dz \right] \right\} \ln|\epsilon_1 - \epsilon_2|\,d\epsilon_1\,d\epsilon_2\,d\theta$$

In order to facilitate subsequent discussion, the above result is manipulated into the following form

$$C_{D_W} S_{REF} = \frac{1}{4\pi^2 L^2(\theta)} \int_0^{2\pi} \int_0^{1} \int_0^{1} \frac{\partial^2}{\partial \epsilon_1^2} A_e(\epsilon_1,\theta) \frac{\partial^2}{\partial \epsilon_2^2} A_e(\epsilon_2,\theta) \ln|\epsilon_1 - \epsilon_2|\,d\epsilon_1\,d\epsilon_2\,d\theta \qquad (23)$$

where

$$A_e(\epsilon,\theta) = A(\epsilon,\theta) - \frac{1}{2}\beta \int_0^{\epsilon} \int_c C_p(\epsilon,\theta) \left[\sin\theta\,dy + \cos\theta\,dz \right] d\epsilon$$

A requirement for this transformation is that

$$A_e'(0,\theta) = A_e'(L,\theta) = 0$$

In accordance with equation 23, the wave drag of a configuration is the average of the wave drag of a series of equivalent bodies of revoluation. The drag of each of these bodies is calculated from a knowledge of its longitudinal distribution of normal cross sectional area. For each equivalent body, these areas are defined to be the frontal projection of the areas and the accumulation of pressure force in the theta direction intercepted on the original configuration by a system of parallel oblique planes each inclined at the given Mach angle. The common trace angle (ϕ) of the system identifies the equivalent body under consideration.

Nacelles are assumed to swallow air supersonically. That is, the duct is operating at a mass flow ratio of unity. Consistent with this assumption, the equivalent body cross sectional area distribution is increased by the oblique projected duct capture area at all stations ahead of the duct which are intercepted by an oblique plane.

Blunt base components are extended (maintaining constant cross sectional area) sufficiently far downstream to prevent flow closure around the base.

In addition to a geometric description, a definition of the pressure distribution acting on the configuration is required. The vortex panel analysis is used for this purpose. The thickness pressures for planar components have tacitly been neglected under the assumption that the surfaces are sufficiently thin that the net pressure coefficient is representative of pressure acting on the oblique section.

Estimation of the wave drag based on equation 23 depends on solution of integrals of the type

$$I = \frac{1}{2\pi} \int_0^1 \int_0^1 G''(x_1)\, G''(x_2) \ln|x_1 - x_2|\, dx_1\, dx_2$$

of a numerically given function G(X). Evaluation of such forms has been studied by Eminton [16,17] for functions having G'(X) continuous on the interval (0,1) and G'(0) = G'(1) = 0. In such situations G'(X) can be expanded in a Fourier sine series. It can then be shown that

$$I = \sum_{N=1}^{\infty} N A_N^2$$

where

$$A_N = \frac{2}{\pi} \int_0^{\pi} G'(x) \sin N\psi \, d\psi$$

Eminton then solved for the value of the Fourier coefficients which result in I being a minimum, subject to the condition that the resulting series for G(X) be exact for an arbitrarily specified set of points o,1, ϵ_i, i = 1,n.

This approach produces the following result

$$I = \frac{4}{\pi}\left[G(1)-G(0)\right]^2 + \pi \sum_{i=1}^{m} \sum_{j=1}^{m} C_i C_j f_{ij}$$

where

$$C_i = G(\epsilon_i) - G(0) - \left[G(1)-G(0)\right]\mu_i$$

$$\mu_i = \frac{1}{\pi}\left\{ \cos^{-1}(1-2\epsilon_i) - 2(1-2\epsilon_i)\sqrt{\epsilon_i(1-\epsilon_i)} \right\}$$

$$\epsilon_i = \frac{i}{n+1} \qquad 1 \le i \le n$$

$$f_{ij} = \left\{ P_{ij} \right\}^{-1}$$

$$P_{ij} = -\frac{1}{2}(\epsilon_i-\epsilon_j)^2 \ln \frac{\epsilon_i+\epsilon_j-2\epsilon_i\epsilon_j+2\sqrt{\epsilon_i\epsilon_j(1-\epsilon_i)(1-\epsilon_j)}}{\epsilon_i+\epsilon_j-2\epsilon_i\epsilon_j-2\sqrt{\epsilon_i\epsilon_j(1-\epsilon_i)(1-\epsilon_j)}}$$

$$+ 2(\epsilon_i+\epsilon_j-\epsilon_i\epsilon_j)\sqrt{\epsilon_i\epsilon_j(1-\epsilon_i)(1-\epsilon_j)}$$

The solution of equation 23 for wave drag is accomplished by use of the following identities.

$$G(\epsilon_i, \theta) = A_e(\epsilon_i, \theta)$$

$$C_{D_w}(\theta) = \frac{I(\theta)}{L^2(\theta)}$$

$$C_{D_w} = \frac{1}{2\pi}\int_0^{2\pi} C_{D_w}(\theta)\,d\theta = \frac{1}{\pi}\int_{-\pi/2}^{\pi/2} C_{D_w}(\theta)\,d\theta$$

Trim Drag

The control surface deflection required to longitudinally balance the configuration at a given angle of attack is calculated from the pitching moment equation:

$$C_m = C_{m_o} + \frac{\partial C_m}{\partial \alpha}\alpha + \frac{\partial C_m}{\partial \delta}\delta_{TRIM} = 0 \qquad (24)$$

or

$$\delta_{TRIM} = \frac{C_{m_o} + \frac{\partial C_m}{\partial \alpha}\alpha}{\frac{\partial C_m}{\partial \delta}}$$

The associated lift coefficient is given by

$$C_L = C_{L_o} + \frac{\partial C_L}{\partial \alpha}\alpha + \frac{\partial C_L}{\partial \delta}\delta_{TRIM} \qquad (25)$$

The trim drag is evaluated using the preceding drag analysis with the control surface deflection angle determined from equation 24.

The lift and pitching moment characteristics appearing in equations (24) and (25) are based on the constant pressure vortex panel simulation described previously. Since this analysis is potential, dynamic pressure losses associated with viscous wake effects have been neglected.

CONCLUSIONS

An aerodynamic configuration evaluation program has been developed and implemented on a time sharing system with an interactive graphics terminal to maximize responsiveness to the preliminary analysis problem

The solution is based on linearized potential theory and treats thickness and attitude problems at subsonic and supersonic speeds. Three dimensional configurations having multiple non-planar surfaces of arbitrary planform and open or closed slender bodies of non-circular contour may be analyzed. Longitudinal and lateral-directional static and rotary derivatives solutions may be generated.

Nominal case computation time of 45 CPU seconds on the CDC 175 for a 200 panel simulation indicates the program provides an efficient analysis for systematically performing various aerodynamic configuration tradeoff and evaluation studies.

REFERENCES

1. Ward, G. N., Linearized Theory of Steady High Speed Flow, Cambridge University Press, 1955.

2. Adams, M. C. and Sears, W. R. "Slender-Body Theory-Review and Extension," Journal of Aeronautical Sciences, February 1953.

3. Hess, J. F. and Smith, A. M. O., "Calculation of Potential Flow About Arbitrary Bodies,"Progress Aeronautical Sciences, Pergramon Press, 1967.

4. Werner, J. and Krenkel, A. R., "Slender Body Theory Programmed for Bodies with Arbitrary Crossection," Polytechnic Institute of New York, Unpublished.

5. Woodward, F. A., "Analysis and Design of Wing-Body Combinations, at Subsonic and Supersonic Speeds," Journal of Aircraft, Vol. 5, No. 6, Nov-Dec., 1968.

6. Householder, A. S., "Unitary Triangularization of a Nonsymmetric Matrix," J. Assoc. Comp. Math 5, 1958.

7. Tulinius, J. et al., "Theoretical Prediction of Airplane Stability Derivatives at Subcritical Speeds," NASA CR-132681, 1975.

8. Schlichting, H., Boundary Layer Theory, Fourth Edition, McGraw-Hill Book Co. Inc. 1958.

9. Eckert, E. R. G., "Survey of Heat Transfer at High Speed," WADC TR-54-70, 1954.

10. Van Driest, E. R., "The Problem of Aerodynamic Heating" Aeronautical Engineering Review, October 1956, pp. 26-41.

11. Goddard, F. E., "Effect of Uniformly Distributed Roughness on Turbulent Skin Friction Drag at Supersonic Speed," Journal Aero/Space Sciences, January 1959, pp. 1-15, 24.

12. Clutter, D. W., "Charts for Determining Skin Friction Coefficients on Smooth and Rough Plates at Mach Numbers up to 5.0 With and Without Heat Transfer," Douglas Aircraft Report No. ES-29074, 1959.

13. Hoerner, S. F., Fluid Dynamic Drag, Published by Author, 148 Busteed Drive, Midland Park, New Jersey, 1958.

14. Hayes, W. D., "Linearized Supersonic Flow," North American Aviation, Inc. Report No. AL-222, 1947.

15. Lomax, H., "The Wave Drag of Arbitrary Configurations in Linearized Flow as Determined by Areas and Forces in Oblique Planes," NACA RM A55A18, 1955.

16. Eminton, E., "On the Minimization and Numerical Evaluation of Wave Drag," RAE Report Aero 2564, 1955.

17. Eminton, E., "On the Numerical Evaluation of the Drag Integral," British R & M 3341, 1963.